DMD Fast Forward. Published on October 23, 2022 as DOI: 10.1124/dmd.122.001000
This article has not been copyedited and formatted. The final version may differ from this version.
Manuscript number: DMD-AR-2022-001000

Title page

Physiologically based pharmacokinetic modeling for quantitative prediction of exposure to a human disproportionate metabolite of the selective $Na_V1.7$ inhibitor DS-1971a, a mixed substrate of cytochrome P450 and aldehyde oxidase, using chimeric mice with humanized liver

Daigo Asano, Koichi Nakamura, Yumi Nishiya, Hideyuki Shiozawa, Hideo Takakusa, Takahiro Shibayama, Shin-ichi Inoue, Tsuyoshi Shinozuka, Takakazu Hamada, Chizuko Yahara, Nobuaki Watanabe, Kouichi Yoshinari

Affiliations

Drug Metabolism and Pharmacokinetics Research Laboratories, Daiichi Sankyo Co., Ltd., Tokyo, Japan (D.A., K.N., N.Y., H.S., H.T., T. Shibayama, S.I., C.Y., N.W.), R&D Planning & Management Department, Daiichi Sankyo Co., Ltd., Tokyo, Japan (T. Shinozuka), Research function, Daiichi Sankyo Co., Ltd., Tokyo, Japan (T.H.), Laboratory of Molecular Toxicology, School of Pharmaceutical Sciences, University of Shizuoka, Shizuoka, Japan (K.Y.)

DMD Fast Forward. Published on October 23, 2022 as DOI: 10.1124/dmd.122.001000
This article has not been copyedited and formatted. The final version may differ from this version.
Manuscript number: DMD-AR-2022-001000

a) Running title: PBPK modeling of a human disproportionate metabolite

b) Corresponding author: Daigo Asano, Drug Metabolism and Pharmacokinetics Research Laboratories, Daiichi Sankyo Co., Ltd., 1-2-58, Hiromachi, Shinagawa-ku, Tokyo 140-8710, Japan, Phone: +81-3-3492-3131, Fax: +81-3-5436-8567
E-mail: asano.daigo.vi@daiichisankyo.co.jp

c) Number of text pages: 32
Number of tables: 6
Number of figures: 6
Number of references: 42
Number of words in the Abstract: 222
Number of words in the Introduction: 746
Number of words in the Discussion: 1500

d) List of abbreviations: AO, aldehyde oxidase; AUC, area under the plasma concentration-time curve; BW, body weight; *CL*, clearance; CL_{int}, intrinsic clearance; C_{max}, maximum plasma concentration; CL_{uint}, unbound intrinsic clearance; DMA, dimethylacetamide; eq., equation; *f*u, unbound fraction; HLM, human liver microsome; HPLC, high-performance liquid chromatography; IVIVE, in vitro to in vivo extrapolation; LC-MS/MS, liquid chromatography-tandem mass spectrometry; *k*a, absorption constant; *k*t, transit constant; M/P ratio, metabolite to parent AUC ratio; P450, cytochrome P450; PBPK, physiologically based pharmacokinetic; PK, pharmacokinetics; *R*b, blood to plasma concentration ratio; SD, standard deviation; TP, transporter; T_{max}, time to reach the maximum plasma concentration; *V*d, distribution volume

DMD Fast Forward. Published on October 23, 2022 as DOI: 10.1124/dmd.122.001000
This article has not been copyedited and formatted. The final version may differ from this version.
Manuscript number: DMD-AR-2022-001000

ABSTRACT

In a previous study on the human mass balance of DS-1971a, a selective $Na_V1.7$ inhibitor, its CYP2C8-dependent metabolite M1 was identified as a human disproportionate metabolite. The present study assessed the usefulness of pharmacokinetic evaluation in chimeric mice grafted with human hepatocytes (PXB-mice) and physiologically based pharmacokinetic (PBPK) simulation of M1. After oral administration of radiolabeled DS-1971a, the most abundant metabolite in the plasma, urine, and feces of PXB-mice was M1, while those of control SCID mice were aldehyde oxidase-related metabolites including M4, suggesting a drastic difference in the metabolism between these mouse strains. From a qualitative perspective, the metabolite profile observed in PXB-mice was remarkably similar to that in humans, but the quantitative evaluation indicated that the area under the curve (AUC) ratio of M1 to DS-1971a (M1/P ratio) was approximately only half of that in humans. A PXB-mouse–derived PBPK model was then constructed to achieve a more accurate prediction, giving an M1/P ratio (1.3) closer to that in humans (1.6) than the observed value in PXB-mice (0.69). In addition, simulated maximum plasma concentration (C_{max}) and AUC values of M1 (3429 ng/mL and 17,116 ng·h/mL, respectively) were similar to those in humans (3180 ng/mL and 18,400 ng·h/mL, respectively). These results suggest that PBPK modeling incorporating pharmacokinetic parameters obtained with PXB-mice is useful for quantitatively predicting exposure to human disproportionate metabolites.

DMD Fast Forward. Published on October 23, 2022 as DOI: 10.1124/dmd.122.001000
This article has not been copyedited and formatted. The final version may differ from this version.
Manuscript number: DMD-AR-2022-001000

Significance statement

The quantitative prediction of human disproportionate metabolites remains challenging. We provided a successful case study on the practical estimation of exposure (C_{max} and AUC) to DS-1971a and its CYP2C8-dependent, human disproportionate metabolite M1 by PBPK simulation utilizing pharmacokinetic parameters obtained from PXB-mice and in vitro kinetics in human liver fractions. This work adds to the growing knowledge regarding metabolite exposure estimation by static and dynamic models.

DMD Fast Forward. Published on October 23, 2022 as DOI: 10.1124/dmd.122.001000
This article has not been copyedited and formatted. The final version may differ from this version.
Manuscript number: DMD-AR-2022-001000

Introduction

Human pharmacokinetics (PK) of parent compounds has been successfully predicted by in vitro to in vivo extrapolation (IVIVE) and allometric methods (Obach et al., 1997; Tang et al., 2007), but the estimation of metabolite PK is still challenging. In fact, there are many cases where human disproportionate metabolites have not been quantitatively characterized until clinical studies.

A few papers indicated that exposure levels of metabolites of cytochrome P450 (P450) substrates such as midazolam, imipramine, (*R*)-4-((4-(((4-((tetrahydrofuran-3-yl)oxy)benzo[*d*]isoxazol-3-yl)oxy)methyl)piperidin-1-yl)methyl)tetrahydro-2*H*-pyran-4-ol (also known as TBPT), and losartan were successfully estimated (Nguyen et al., 2016; Obach et al., 2018; Callegari et al., 2020), while even fewer papers described successful attempts for substrates where non-P450 enzymes were involved. Two approaches can predict metabolite exposure: static and dynamic models. Although static models enable a point-in-time calculation of metabolite-to-parent AUC ratios (M/P ratios), dynamic models provide us with not only M/P ratios, but also important PK parameters including maximum plasma concentration (C_{max}) and the area under the curve (AUC) values. Dynamic models include the physiologically based pharmacokinetic (PBPK) models in which various kinds of animal and human physiological parameters, such as blood flow and organ volumes, are involved. Since substantial information about physiology and complex systems is required for the construction of a full PBPK model, researchers frequently utilize commercially available software, including Simcyp™ (Nguyen et al., 2016; Obach et al., 2018) and Gastroplus® (Yamada et al., 2020). Meanwhile, customized PBPK models (Gill et al., 2013; Ito et al., 2020) are also developed on a fit-for-purpose basis.

PXB-mouse® are chimeric mice prepared by the injection of human hepatocytes into the spleen of immunodeficient mice. More than 70% of liver cells in PXB-mice are replaced with human hepatocytes and various kinds of human metabolizing enzymes and transporters are expressed in the liver of PXB-mice (Okumura et al., 2007; Hasegawa et al., 2012; Tateno et al., 2013). PXB-mice can be used for estimating human PK parameters by the allometric

DMD Fast Forward. Published on October 23, 2022 as DOI: 10.1124/dmd.122.001000
This article has not been copyedited and formatted. The final version may differ from this version.
Manuscript number: DMD-AR-2022-001000

scaling method (Sanoh et al., 2015) and in vivo metabolite profiles in PXB-mice qualitatively reflect those in humans (Kato et al., 2020). Additionally, urinary and biliary excretion of metabolites in PXB-mice reflects that in humans (Sanoh et al., 2012; Kato et al., 2020). Meanwhile, caution should be paid to the influence of the remaining mouse hepatocytes on experimental results, and the accuracy of human metabolite prediction would depend on a case-by-case basis, as illustrated by the detection of metabolites produced by remaining mouse hepatocytes (Kamimura et al., 2010).

DS-1971a is a selective voltage-gated sodium channel (Na_v)1.7 inhibitor under a clinical trial for neuropathic pain (Shinozuka et al., 2020). Nonclinical evaluation indicated that more than 90% of radiolabeled DS-1971a was orally absorbed in male ICR mice and monkeys, and various kinds of oxidized metabolites with species differences in abundance were observed (Asano et al., 2021). Male ICR mice had the highest exposure to the aldehyde oxidase (AO)-dependent metabolite, M4, while the P450-produced metabolite, M2, was the predominant metabolite in male monkeys (Fig. 1). Thus, DS-1971a was identified as a mixed AO and P450 substrate. In vitro incubation study with human liver S9 in the presence of NADPH indicated that M1, a regioisomer of M2, was the potential major metabolite in humans.

A human mass balance study of radiolabeled DS-1971a in the fed condition demonstrated that more than 70% of the dose was absorbed and the predominant metabolite was M1 in human plasma, urine, and feces (Asano et al., 2022). The exposure level of M1 in human plasma was 1.5-fold higher than that of the parent compound (DS-1971a) and M1 exposure in animals used for safety assessments (mice and monkeys) was much smaller than that in humans, so M1 was found to be a human disproportionate metabolite. In addition, incubation studies with human liver microsomes (HLMs) pretreated with P450-specific inhibitors and with recombinant P450 have indicated that CYP2C8 plays a key role in M1 formation (Asano et al., 2022).

Although previous studies on M1 formation in animals and humans suggested that M1 was a human disproportionate metabolite from a retrospective view, a critical question

DMD Fast Forward. Published on October 23, 2022 as DOI: 10.1124/dmd.122.001000
This article has not been copyedited and formatted. The final version may differ from this version.

remains: How can the human exposure level of M1 as a human disproportionate metabolite be estimated before clinical trials? To answer this question, we performed PK evaluation in PXB-mice, which are likely the only animal species possessing human-like metabolic activity toward DS-1971a. Further, a PBPK model was constructed to predict the exposure levels of DS-1971a and M1. We here demonstrate the usefulness of the PBPK model derived from PXB-mice for estimating exposure of a human disproportionate metabolite.

DMD Fast Forward. Published on October 23, 2022 as DOI: 10.1124/dmd.122.001000
This article has not been copyedited and formatted. The final version may differ from this version.
Manuscript number: DMD-AR-2022-001000

Materials and Methods

Chemicals and Reagents

DS-1971a (5-chloro-2-fluoro-4-{[(1*S*,2*R*)-2-(1-methyl-1*H*-pyrazol-5-yl)cyclohexyl]oxy}-*N*-(pyrimidin-4-yl)benzenesulfonamide), a stable-isotope-labeled racemic mixture of DS-1971a (5-chloro-2-fluoro-4-{[(1*RS*,2*SR*)-2-[1-(^{13}C,$^{2}H_3$)methyl-1*H*-pyrazol-5-yl]cyclohexyl]oxy}-*N*-(pyrimidin-4-yl)benzenesulfonamide), M1 (5-chloro-2-fluoro-4-{[(1*S*,2*R*,5*S*)-5-hydroxy-2-(1-methyl-1*H*-pyrazol-5-yl)cyclohexyl]oxy}-*N*-(pyrimidin-4-yl)benzenesulfonamide), M2 (5-chloro-2-fluoro-4-{[(1*S*,2*R*,4*R*)-4-hydroxy-2-(1-methyl-1*H*-pyrazol-5-yl)cyclohexyl]oxy}-*N*-(pyrimidin-4-yl)benzenesulfonamide), M3 (5-chloro-2-fluoro-4-{[(1*S*,2*R*,4*S*)-4-hydroxy-2-(1-methyl-1*H*-pyrazol-5-yl)cyclohexyl]oxy}-*N*-(pyrimidin-4-yl)benzenesulfonamide), M4 (5-chloro-2-fluoro-4-{[(1*S*,2*R*)-2-(1-methyl-1*H*-pyrazol-5-yl)cyclohexyl]oxy}-*N*-(2-oxo-1,2-dihydropyrimidin-4-yl)benzenesulfonamide), a racemic mixture of M5 (5-chloro-2-fluoro-4-{[(1*RS*,2*SR*,5*SR*)-5-hydroxy-2-(1-methyl-1*H*-pyrazol-5-yl)cyclohexyl]oxy}-*N*-(pyrimidin-4-yl)benzenesulfonamide), M6 (5-chloro-2-fluoro-4-{[(1*S*,2*R*)-2-(4-hydroxy-1-methyl-1*H*-pyrazol-5-yl)cyclohexyl]oxy}-*N*-(pyrimidin-4-yl)benzenesulfonamide), a racemic mixture of M7 (5-chloro-2-fluoro-4-{[(1*RS*,2*SR*,4*RS*)-4-hydroxy-2-(1-methyl-1*H*-pyrazol-5-yl)cyclohexyl]oxy}-*N*-(2-oxo-1,2-dihydropyrimidin-4-yl)benzenesulfonamide), a racemic mixture of M8 (5-chloro-2-fluoro-4-{[(1*RS*,2*SR*,4*SR*)-4-hydroxy-2-(1-methyl-1*H*-pyrazol-5-yl)cyclohexyl]oxy}-*N*-(2-oxo-1,2-dihydropyrimidin-4-yl)benzenesulfonamide), a racemic mixture of M9 (5-chloro-2-fluoro-4-{[(1*RS*,2*SR*,5*RS*)-5-hydroxy-2-(1-methyl-1*H*-pyrazol-5-yl)cyclohexyl]oxy}-*N*-(2-oxo-1,2-dihydropyrimidin-4-yl)benzenesulfonamide), a racemic mixture of M10 (5-chloro-2-fluoro-4-{[(1*RS*,2*SR*,5*SR*)-5-hydroxy-2-(1-methyl-1*H*-pyrazol-5-yl)cyclohexyl]oxy}-*N*-(2-oxo-1,2-dihydropyrimidin-4-yl)benzenesulfonamide), M11 (5-chloro-2-fluoro-4-{[(1*S*,2*R*)-2-(1*H*-pyrazol-5-yl)cyclohexyl]oxy}-*N*-(pyrimidin-4-yl)benzenesulfonamide), M12 (5-chloro-2-fluoro-4-({(1*S*,2*S*)-2-[(4*R*)-4-hydroxy-1-methyl-5-oxo-4,5-dihydro-1*H*-pyrazol-4-yl]cyclohexyl}oxy)-*N*-(pyrimidin-4-yl)benzenesulfonamide), and M13 (5-chloro-2-fluoro-4-({(1*S*,2*S*)-2-[(4*S*)-4-hydroxy-1-methyl-5-oxo-4,5-dihydro-1*H*-pyrazol-4-yl]cyclohexyl}oxy)-*N*-

DMD Fast Forward. Published on October 23, 2022 as DOI: 10.1124/dmd.122.001000
This article has not been copyedited and formatted. The final version may differ from this version.
Manuscript number: DMD-AR-2022-001000

(pyrimidin-4-yl)benzenesulfonamide) were synthesized at Daiichi Sankyo Co., Ltd. (Tokyo, Japan). [^{3}H]DS-1971a (Fig. 1C, 999 GBq/mmol, 37 MBq/mL in ethanol; radiochemical purity, 99%) was purchased from Sekisui Medical Co., Ltd. (Tokyo, Japan). Pooled liver microsome and S9 from humans was purchased from XenoTech (Kansas City, KS). Potassium phosphate buffer (KPB; pH 7.4), and NADPH-regenerating system solutions A and B were purchased from Corning (Woburn, MA). Fresh human blood and plasma were provided by Daiichi Sankyo Co., Ltd. (Tokyo, Japan). Dimethylacetamide (DMA) was obtained from Nacalai Tesque (Kyoto, Japan). Saline was obtained from Otsuka Pharmaceutical Factory, Inc. (Tokushima, Japan). PXB cells whose replacement index were around 90%, were purchased from PhoenixBio (Hiroshima, Japan).

Animals

Animal experiments were approved by the Institutional Animal Care and Use Committee, and performed in accordance with the animal welfare guidelines of Daiichi Sankyo Co., Ltd., which is accredited by AAALAC International. Male CB-17 SCID mice (10 weeks old) were obtained from Charles River Laboratories Japan, Inc. (Yokohama, Japan). Male PXB-mice (12–18 weeks) whose replacement index were around 90%, were purchased from PhoenixBio (Hiroshima, Japan).

PK Study of DS-1971a and M1 in SCID Mice and PXB-mice

DS-1971a dissolved in vehicle (10% DMA and 90% saline) was intravenously and orally administered to fasted SCID mice and PXB-mice (N = 3) at a dose of 10 mg/5 mL/kg. M1 dissolved in the same vehicle was intravenously injected into fasted PXB-mice (N = 3) at a dose of 1 mg/5 mL/kg. Plasma samples were collected 0.083 and/or 0.25, 0.5, 1, 2, 4, 7, and 24 h later. Extraction and LC-MS/MS measurement were performed as previously described (Asano et al., 2021). PK parameters (i.e., total plasma clearance and plasma distribution volume in a steady state (Vd_{ss}) after intravenous administration, maximum plasma

DMD Fast Forward. Published on October 23, 2022 as DOI: 10.1124/dmd.122.001000
This article has not been copyedited and formatted. The final version may differ from this version.
Manuscript number: DMD-AR-2022-001000

concentration (C_{max}), time to reach the maximum plasma concentration (T_{max}) and apparent oral plasma clearance after oral administration, and area under the curve from the time of dosing to the time of the last observation (AUC) after both intravenous and oral administration) were calculated based on a non-compartmental analysis technique using WinNonlin 6.3 (Certara, Princeton, NJ). Oral bioavailability of DS-1971a was calculated by dividing the AUC of DS-1971a after oral administration by that after intravenous administration and multiplying times 100. M1/P ratio was obtained by dividing the AUC of M1 by the AUC of DS-1971a after oral dosing.

Calculation of Dose-Normalized AUC of M1

Dose-normalized AUC in various species were calculated as follows.

$$\text{Normalized AUC} = \text{observed AUC} \times \frac{\text{oral dose in humans} \div \text{human BW}}{\text{oral dose in various species}} \quad (1)$$

Here, oral dose in humans is 400 mg and human BW represents body weight of 70 kg for humans (Davies and Morris, 1993). Oral dose (3–10 mg/kg) and observed AUC in ICR mice, monkeys, rats, and dogs are cited from Asano et al. (2021, 2022), and those in SCID mice and PXB-mice are described in this manuscript.

Mass Balance Study of Radiolabeled DS-1971a in SCID Mice and PXB-mice

[^{3}H]DS-1971a dissolved in vehicle (10% DMA and 90% saline) was orally administered to fasted SCID mice and PXB-mice (N = 3) at a dose of 10 mg/5 mL/kg. Urine and feces were collected at 0–72 h post-administration. Fifty microliters of urine or homogenized feces was mixed with 2 mL of tissue solubilizer Solvable (PerkinElmer, Waltham, MA) and 10 mL of the scintillator Hionic-fluor, and radioactivity was measured using a Tri-Carb 3110TR liquid scintillation counter (PerkinElmer). The excretion ratio of radioactivity in urine and feces (% of dose) was calculated by dividing the excreted radioactivity by the administered radioactivity.

Metabolite Detection in Plasma, Liver, Urine, and Feces of SCID mice and PXB-mice,

DMD Fast Forward. Published on October 23, 2022 as DOI: 10.1124/dmd.122.001000
This article has not been copyedited and formatted. The final version may differ from this version.
Manuscript number: DMD-AR-2022-001000

and Calculation of Urinary, Biliary, and Metabolic Clearance in PXB-mice

After oral administration of [^{3}H]DS-1971a dissolved in vehicle (10% DMA and 90% saline) to fasted SCID mice and PXB-mice (N = 3) at a dose of 10 mg/5 mL/kg, plasma and liver samples were collected from mice 1 h later. In addition, urinary and fecal samples collected in the mass balance study described above were used for metabolite detection. Extraction and radio-HPLC analysis of collected plasma, liver, urine, and feces were performed as previously described (Asano et al., 2021). Based on the radiochromatograms of urinary and fecal extracts, the composition ratio and amounts of DS-1971a and M1 excreted into urine and feces were calculated. Throughout the manuscript, second subscripts “p” and “m” of abbreviations represent parent and metabolite, respectively. The hepatic biliary plasma clearance (*CL*bp and *CL*bm), renal plasma clearance (*CL*rp and *CL*rm), and hepatic metabolic plasma clearance (*CL*mp and *CL*mm) of DS-1971a and M1 in PXB-mice were calculated as follows:

$$CL\text{bp in PXB-mice (mL/min/kg)} = \text{Apparent oral plasma clearance of DS-1971a} \times \frac{\text{Amount of DS-1971a excreted in feces}}{\text{Dose}} \quad (2)$$

$$CL\text{bm in PXB-mice (mL/min/kg)} = \text{Apparent oral plasma clearance of M1} \times \frac{\text{Amount of M1 excreted in feces}}{\text{Dose}} \quad (3)$$

$$CL\text{rp in PXB-mice (mL/min/kg)} = \frac{\text{Amount of DS-1971a excreted in urine}}{\text{Plasma AUC of DS-1971a}} \quad (4)$$

$$CL\text{rm in PXB-mice (mL/min/kg)} = \frac{\text{Amount of M1 excreted in urine}}{\text{Plasma AUC of M1}} \quad (5)$$

$$CL\text{mp in PXB-mice (mL/min/kg)} = \text{Total plasma clearance of DS-1971a } (CL\text{p,total}) - CL\text{bp} - CL\text{rp} \quad (6)$$

$$CL\text{mm in PXB-mice (mL/min/kg)} = \text{Total plasma clearance of M1 } (CL\text{m,total}) - CL\text{bm} - CL\text{rm} \quad (7)$$

Note that biliary plasma clearance (*CL*bp and *CL*bm) were calculated based on previous reports (Yang et al., 2009) with some modifications, assuming that the fecal recovery of DS-1971a and M1 was equal to the biliary excretion because no further metabolism of either compound was confirmed when they were incubated for 24 h with fecal homogenates from PXB-mice (data not shown), and both fraction absorbed (*F*a) and intestinal availability (*F*g) of DS-1971a in PXB-mice were calculated to be 1.0 (described later). Total plasma clearance (*CL*p,total and *CL*m,total), which were determined in intravenous PK study of DS-1971a and

DMD Fast Forward. Published on October 23, 2022 as DOI: 10.1124/dmd.122.001000
This article has not been copyedited and formatted. The final version may differ from this version.
Manuscript number: DMD-AR-2022-001000

M1, were assumed to be the sum of biliary plasma clearance (*CL*bp and *CL*bm), renal plasma clearance (*CL*rp and *CL*rm), and hepatic metabolic plasma clearance (*CL*mp and *CL*mm).

Human clearance and Vd_{ss} Estimation by Single Species Allometric Scaling of PK Parameters in PXB-mice

Based on a previous report (Sanoh et al., 2015), the plasma clearance (*CL*bp, *CL*bm, *CL*rp, *CL*rm, *CL*mp, and *CL*mm) and plasma volume of distribution in a steady state (Vd_{ss}) of DS-1971a and M1 in humans were estimated using the following equations.

$$\text{Human plasma } CL\text{s} = \text{PXB-mouse plasma } CL\text{s} \times (\text{human BW} / \text{PXB-mouse BW})^{0.814} \quad (8)$$

$$\text{Human plasma } Vd_{ss} = \text{PXB-mouse plasma } Vd_{ss} \times (\text{human BW} / \text{PXB-mouse BW})^{0.9} \quad (9)$$

Here, BW represents body weight: 70 kg for humans (Davies and Morris, 1993) and 0.020 kg for PXB-mice (the measured value of the purchased PXB-mice).

Measurement of Concentration-Based *R*b Values of DS-1971a and M1

DS-1971a or M1 (1 μM) was incubated in human blood at 37°C for 5 min. The final concentration of organic solvent was less than 1.0%. Incubated human blood samples were centrifuged at 21,600 *g* for 3 min to separate supernatant plasma fractions. DS-1971a and M1 concentrations in the separated supernatant plasma samples from the incubated blood (referred to as “supernatant sample”) were quantified by LC-MS/MS. Concentration-based blood to plasma ratios of DS-1971a (*R*bp) and M1 (*R*bm) were calculated by dividing the tested concentration (1 μM) by that in “supernatant sample,” assuming no degradation during incubation.

Calculation of Hepatic Availability of DS-1971a (*F*h,p) and M1 (*F*h,m) in PXB-mice and Humans

Hepatic availability of DS-1971a and M1 (*F*h,p and *F*h,m) was calculated based on the following equations:

DMD Fast Forward. Published on October 23, 2022 as DOI: 10.1124/dmd.122.001000
This article has not been copyedited and formatted. The final version may differ from this version.
Manuscript number: DMD-AR-2022-001000

$$F\text{h,p} = 1 - \frac{CL\text{mp} + CL\text{bp}}{R\text{bp} \times Q\text{h}} \quad (10)$$

$$F\text{h,m} = 1 - \frac{CL\text{mm} + CL\text{bm}}{R\text{bm} \times Q\text{h}} \quad (11)$$

where Qh represents hepatic blood flow of 90 mL/min/kg for PXB-mice and 21 mL/min/kg for humans (Davies and Morris, 1993) and hepatic plasma clearance was assumed to be the total of biliary (CLbp and CLbm) and metabolic plasma clearance (CLmp and CLmm).

Measurement of Liver Kp Value in PXB-mice

PXB-mouse plasma and liver samples collected for the metabolite detection experiment were used for measurement of liver Kp values. Based on the radioactive concentration of the plasma and liver homogenates measured using a Tri-Carb 3110TR liquid scintillation counter (PerkinElmer, Waltham, MA) and radiochromatograms obtained in the metabolite detection experiment, liver-plasma partition coefficients of DS-1971a (Kphp) and M1 (Kphm) were calculated by dividing the liver concentrations of DS-1971a and M1 by their plasma concentrations, respectively.

Incubation of DS-1971a with HLM

DS-1971a (0.1, 0.3, 1, 3, 10, and 30 μM) was incubated with HLM (0.5 mg protein/mL in 100 mM KPB, pH 7.4) in the presence of the NADPH-regenerating system at 37°C for 10 min in triplicate and the concentrations of DS-1971a and M1 were determined by LC-MS/MS. The final concentration of organic solvent was less than 1.0%. The depletion rate for DS-1971a and formation rate for M1 were calculated by dividing the measured concentrations of both compounds by the protein concentration and incubation time using Microsoft Excel 2010. Based on the obtained depletion or formation rate for DS-1971a and M1, K_m and V_{max} were determined by a simple E_{max} model (model 101) using WinNonlin 6.3 based on the following equation.

$$E = \frac{E_{max} \times C}{C + EC_{50}} \quad (12)$$

DMD Fast Forward. Published on October 23, 2022 as DOI: 10.1124/dmd.122.001000
This article has not been copyedited and formatted. The final version may differ from this version.
Manuscript number: DMD-AR-2022-001000

where E, C, EC_{50}, and E_{max} represent metabolic reaction velocity, DS-1971a concentration, K_m, and V_{max} as per the Michaelis–Menten equation, respectively.

Intrinsic clearance (CL_{int}) for DS-1971a depletion and M1 formation was calculated by dividing the V_{max} values by the corresponding K_m values.

Protein Binding of DS-1971a in Human Liver Microsomes and S9

The free fractions of DS-1971a in human liver microsomes (0.5 mg/mL in 100 mM KPB, pH 7.4) and S9 (1 mg/mL in 100 mM KPB, pH 7.4) were determined in triplicate as *f*u,mic and *f*u,S9, respectively, based on the previously described method (Shinozuka et al., 2020).

Estimation of Fractional Metabolite Clearance and Plasma M1/P Ratio by the Static Model

Since no metabolism of DS-1971a into M1 in human intestinal microsomes and S9 was observed (data not shown), the M1-to-parent plasma AUC ratio (M1/P ratio) was calculated without consideration of gut metabolism based on the following equation (Nguyen et al., 2016; Obach et al., 2018):

$$\frac{\text{AUCm}}{\text{AUCp}} = \frac{F\text{h,m} \times \text{f}CL\text{,m} \times CL\text{p,total}}{F\text{h,p} \times CL\text{m,total}} \times \frac{\text{MW of metabolite (M1 = 481)}}{\text{MW of parent (DS-1971a = 465)}} \quad (13)$$

Here, AUCp, AUCm, *F*h,p, *F*h,m, *CL*p,total, *CL*m,total, and f*CL*,m represent plasma AUC of parent (DS-1971a), plasma AUC of metabolite (M1), hepatic availability of DS-1971a, hepatic availability of M1, total plasma clearance of parent (DS-1971a), total plasma clearance of metabolite (M1), and the fraction of parent (DS-1971a) clearance through hepatic metabolite (M1) formation, respectively. f*CL*,m in PXB-mice was obtained by measuring the total excretion (% of dose/100) of M1 into urine and feces after the oral administration of radiolabeled DS-1971a to PXB-mice. Meanwhile, f*CL*,m in humans was calculated as follows:

f*CL*,m in humans = CL_{uint} by P450 for M1 formation in HLM × mSF ÷ (CL_{uint} by P450 for DS-1971a depletion in HLM × mSF + CL_{uint} by AO for DS-1971a depletion in human liver S9 ×

DMD Fast Forward. Published on October 23, 2022 as DOI: 10.1124/dmd.122.001000
This article has not been copyedited and formatted. The final version may differ from this version.
Manuscript number: DMD-AR-2022-001000

sSF) (14)

Here, CL_{uint} represents unbound intrinsic clearance. CL_{uint} by P450 for M1 formation and CL_{uint} by P450 for DS-1971a depletion were calculated by dividing respective V_{max} values by K_m values corrected for the $f_{u,mic}$ of the incubation. CL_{uint} by AO was calculated by correcting the previously reported $CL_{int,AO}$ value for the $f_{u,S9}$ of the incubation (Asano et al., 2021). mSF and sSF represent physiological scaling factors for human liver microsomal proteins (46 mg protein/g liver) (Zhou et al., 2002) and S9 proteins (121 mg protein/g liver) (Houston and Galetin, 2008), respectively. Note that biliary and urinary clearance of DS-1971a were not taken into account for this calculation because of the negligible (less than 1%) excretion into bile and urine as an intact form in PXB-mouse mass balance study (described later).

Simulation of PK Profiles of DS-1971a and M1 in PXB-mice and Humans Using Dynamic PBPK Models

Development of PBPK models and simulations were all performed by the Phoenix model using WinNonlin 6.3. The following parameters were used for PBPK models.

[Appendix]

Ag1	drug amount in the upper intestine
Ag2	drug amount in the lower intestine
blood-*CL*rm	renal blood clearance of M1
blood-*CL*rp	renal blood clearance of DS-1971a
Cbm	blood concentration of M1
Cbp	blood concentration of DS-1971a
Chm	hepatic concentration of M1
Chp	hepatic concentration of DS-1971a
$CL_{int,bm}$	biliary blood intrinsic clearance of M1
$CL_{int,bp}$	biliary blood intrinsic clearance of DS-1971a
$CL_{int,mp}$	metabolic blood intrinsic clearance of DS-1971a
f*CL*,m	fraction of the clearance of DS-1971a that yields M1

DMD Fast Forward. Published on October 23, 2022 as DOI: 10.1124/dmd.122.001000
This article has not been copyedited and formatted. The final version may differ from this version.
Manuscript number: DMD-AR-2022-001000

*F*g	intestinal availability
*f*um	unbound fraction of M1 in plasma
*f*up	unbound fraction of DS-1971a in plasma
*k*a1	absorption constant-1
*k*a2	absorption constant-2
*K*phm	liver-to-plasma ratio of M1
*K*php	liver-to-plasma ratio of DS-1971a
*k*t	transit constant
MWm	molecular weight of M1
MWp	molecular weight of DS-1971a
*Q*h	hepatic blood flow
*R*bm	blood-to-plasma concentration ratio of M1
*R*bp	blood-to-plasma concentration ratio of DS-1971a
*V*h	liver volume
*V*1m	blood-based extrahepatic distribution volume of M1
*V*1p	blood-based extrahepatic distribution volume of DS-1971a

[Mass balance formulas]

The minimal PBPK model (Fig. 2) was developed based on a previous report (Ito et al., 2020) with some modifications to simulate PK profiles after oral administration of DS-1971a at a dose of 0.2 mg for PXB-mice and 400 mg for humans. The following mass balance formulas were simultaneously solved by Phoenix model using WinNonlin 6.3. The inputted value of each parameter for PXB-mice and humans are described in Supplementary Table S4 and Table 5, respectively.

- Upper intestinal compartment of DS-1971a

$$\frac{dAg1}{dt} = - ka1 \times Ag1 - kt \times Ag1 \quad (15)$$

DMD Fast Forward. Published on October 23, 2022 as DOI: 10.1124/dmd.122.001000
This article has not been copyedited and formatted. The final version may differ from this version.
Manuscript number: DMD-AR-2022-001000

- Lower intestinal compartment of DS-1971a

$$\frac{dAg2}{dt} = kt \times Ag1 - ka2 \times Ag2 \quad (16)$$

- Liver compartment of DS-1971a

$$\frac{dChp}{dt} \times Vh = Ag1 \times Fg \times ka1 + Ag2 \times Fg \times ka2 - CL_{int,mp} \times \left(\frac{Chp}{Kphp} \times fup\right) - Qh \times \left(\frac{Chp}{Kphp} \times Rbp - Cbp\right) - CL_{int,bp} \times \left(\frac{Chp}{Kphp} \times fup\right) \quad (17)$$

- Blood compartment of DS-1971a

$$\frac{dCbp}{dt} \times V1p = Qh \times \left(\frac{Chp}{Kphp} \times Rbp - Cbp\right) - blood\text{-}CLrp \times Cbp \quad (18)$$

- Liver compartment of M1

$$\frac{dChm}{dt} \times Vh = fCL,m \times CL_{int,mp} \times \left(\frac{Chp}{Kphp} \times fup\right) \times \frac{MWm}{MWp} - Qh \times \left(\frac{Chm}{Kphm} \times Rbm - Cbm\right) - CL_{int,bm} \times \left(\frac{Chm}{Kphm} \times fum\right) \quad (19)$$

- Blood compartment of M1

$$\frac{dCbm}{dt} \times V1m = Qh \times \left(\frac{Chm}{Kphm} \times Rbm - Cbm\right) - blood\text{-}CLrm \times Cbm \quad (20)$$

Note that hepatic metabolism of M1 is not included in equation (eq.) (19) because M1 was reported to be metabolically stable against human liver microsomes and S9 (Asano et al., 2022), indicating that the only elimination pathways of M1 are its biliary and urinary excretion in its unchanged form.

[Calculation of plasma concentrations, C_{max} and AUC]

Since mass balance formulas were described as blood-based parameters, plasma concentrations of DS-1971a and M1 were calculated as follows.

・Plasma concentration of DS-1971a = $\frac{Cbp}{Rbp}$ (21)

・Plasma concentration of M1 = $\frac{Cbm}{Rbm}$ (22)

PK parameters were calculated by non-compartmental analysis of the simulated plasma PK profiles of DS-1971a and M1 in PXB-mice and humans using WinNonlin 6.3.

[Acquisition of parameters used in mass balance formulas]

DMD Fast Forward. Published on October 23, 2022 as DOI: 10.1124/dmd.122.001000
This article has not been copyedited and formatted. The final version may differ from this version.
Manuscript number: DMD-AR-2022-001000

The values of *f*um, *f*up, *Q*h, and *V*h are cited from previous reports (Davies and Morris, 1993, Sinozuka et al., 2020; Asano et al., 2022). f*CL*,m, *K*phm, *K*php, *R*bm, and *R*bp values were experimentally obtained (described before). Other parameters besides certain variables (Ag1, Ag2, Cbm, Cbp, Chm and Chp) were acquired as follows. It is noted that BW represents body weight: 70 kg for humans (Davies and Morris, 1993) and 0.020 kg for PXB-mice (the measured value of the purchased PXB-mice).

- **blood-*CL*rp and blood-*CL*rm**

Renal plasma clearance (*CL*rp and *CL*rm) were divided by *R*b values (*R*bp and *R*bm) with unit conversion.

$$\text{blood-}CL\text{rp (L/h)} = \frac{CL\text{rp}}{R\text{bp}} \times \text{BW} \times 60\ \text{min} \div 1000 \quad (23)$$

$$\text{blood-}CL\text{rm (L/h)} = \frac{CL\text{rm}}{R\text{bm}} \times \text{BW} \times 60\ \text{min} \div 1000 \quad (24)$$

- ***CL*$_{int}$,bm, *CL*$_{int}$,bp, and *CL*$_{int}$,mp**

CL$_{int}$,mp, *CL*$_{int}$,bp, and *CL*$_{int}$,bm were calculated based on the well-stirred model with unit conversion as follows:

$$CL_{int},\text{bm (L/h)} = \frac{CL\text{bm}}{f\text{um}} \times \frac{Q\text{h}}{(Q\text{h} - CL\text{bm} / R\text{bm})} \times \text{BW} \times 60\ \text{min} \div 1000 \quad (25)$$

$$CL_{int},\text{bp (L/h)} = \frac{CL\text{bp}}{f\text{up}} \times \frac{Q\text{h}}{(Q\text{h} - CL\text{bp} / R\text{bp})} \times \text{BW} \times 60\ \text{min} \div 1000 \quad (26)$$

$$CL_{int},\text{mp (L/h)} = \frac{CL\text{mp}}{f\text{up}} \times \frac{Q\text{h}}{(Q\text{h} - CL\text{mp} / R\text{bp})} \times \text{BW} \times 60\ \text{min} \div 1000 \quad (27)$$

- ***F*a and *F*g**

Our previous work (Asano et al., 2021) indicated that 95% and 4.2% of the doses were recovered in bile and urine, respectively, after the oral administration of radiolabeled DS-1971a to mice, suggesting that the oral absorption of DS-1971a is more than 95% in mice. In addition, oral absorption in monkeys can be calculated to be 100% based on the urinary (35% and 38%) and total recovery (91% and 95%) after intravenous and oral administration (Asano et al., 2021) using a previously reported equation (Pleiss, 2005) with modification.

DMD Fast Forward. Published on October 23, 2022 as DOI: 10.1124/dmd.122.001000
This article has not been copyedited and formatted. The final version may differ from this version.
Manuscript number: DMD-AR-2022-001000

$$\text{Oral absorption} = \frac{\text{Urinary recovery after oral administration}}{\text{Urinary recovery after intravenous administration}} \times \frac{\text{Total recovery after intravenous administration}}{\text{Total recovery after oral administration}} \times 100 \quad (28)$$

Based on this evidence and the fact that no metabolism of DS-1971a with human intestinal microsomes and S9 was observed (data not shown), both fraction absorbed (*F*a) and intestinal availability (*F*g) were assumed to be 1.0. These assumptions were also applicable to *F*a and *F*g values in PXB-mice both because *F*h,p in PXB-mice can be calculated to be 0.59 by eq. (10) based on the observed *CL*mp of 20 mL/min/kg, *CL*bp of 0.27 mL/min/kg, *R*b value of DS-1971a of 0.55 (Supplementary Tables S3–S4, described later), and *Q*h value of 90 mL/min/kg in mice (Davies and Morris, 1993), and because the *F*a × *F*g value can be calculated to be 1.0 by the following equation.

$$F\text{a} \times F\text{g in PXB-mice} = \frac{\text{Oral bioavailability, pxb}}{100 \times F\text{h,p, pxb}} \quad (29)$$

where observed oral bioavailability and *F*h,p in PXB-mice were 60% (Supplementary Table S2, described later) and 0.59 (calculated above), respectively.

Thus, both *F*a and *F*g values were assumed to be 1.0 in the PBPK model and the initial value of Ag1 (Ag1 value at time 0 h) was equal to the oral doses (0.2 mg for PXB-mice and 400 mg for humans) by multiplying the oral doses by an *F*a value of 1.0.

- ***k*a1, *k*a2, and *k*t**

The values of *k*a1, *k*a2, and *k*t for PXB-mice were derived by fitting the plasma concentration of DS-1971a in PXB mice to the above PBPK model with multiplicative error using WinNonlin 6.3. *k*a1 and *k*a2 values for humans were estimated from the permeability value in MDCK II cells (described later). *k*t value for humans was calculated based on the following equation (Yu and Amidon,1998).

$$k\text{t in humans} = \frac{\text{Number of intestinal compartment (N = 2)}}{\text{Intestinal transit time (3.5 h)}} \quad (30)$$

Supplementary *k*a1, *k*a2 and *k*t values for humans were obtained in the same way as those for PXB-mice.

- **MWm and MWp**

Molecular weights of M1 and DS-1971a (MWm and MWp) were calculated to be 481 and 465

DMD Fast Forward. Published on October 23, 2022 as DOI: 10.1124/dmd.122.001000
This article has not been copyedited and formatted. The final version may differ from this version.
Manuscript number: DMD-AR-2022-001000

g/mole, respectively.

- ***V*1m and *V*1p**

Blood distribution volumes (*V*d) other than liver (*V*d of blood components were called *V*1p for DS-1971a and *V*1m for M1) were calculated as in a previous report (Ito et al., 2020) using the following equation.

$$V1p \text{ or } V1m \text{ (L)} = \frac{Vd_{ss} \times BW}{(Rbp \text{ or } Rbm)} - \frac{Vh \times (Kphp \text{ or } Kphm)}{(Rbp \text{ or } Rbm)} \times (Fh,p \text{ or } Fh,m) \quad (31)$$

The values of body weight (BW), liver volume (*V*h), and *Q*h used were 0.02 kg, 0.0013 L, and 90 mL/min/kg for PXB-mice and 70 kg, 1.7 L, and 21 mL/min/kg for humans, respectively (Davies and Morris, 1993).

Membrane Permeability of DS-1971a in MDCK II Cells, and Estimation of Absorption Constants-1 and -2 in Humans

Apparent permeability (P_{app}) of DS-1971a was assayed in sextuplicate using MDCK II cells, as previously reported (Furukawa et al., 2021). Absorption constants-1 and -2 (*k*a1 and *k*a2) in humans were estimated based on the following equation.

$$ka1 \text{ and } ka2 \text{ in humans} = \frac{2 \times P_{eff}}{R} \text{ (Yu and Amidon, 1999)} \quad (32)$$

where R means small intestinal radius (1.75 cm) and P_{eff} represents effective permeability, which was calculated from P_{app} by SimCYP™ (Certara, Princeton, NJ) based on the following equation (Tchaparian et al., 2008).

$$\log10 [P_{eff} \text{ in humans}] = 1.0117 \times \log10 [P_{app} \text{ in MDCK II cells}] - 0.912 \quad (33)$$

Determination of LogD Values of DS-1971a, M1, M2, and M4

LogD values of DS-1971, M1, M2, or M4 were assayed as previously reported (Nagata, 2009). In brief, DS-1971a, M1, M2, or M4 (1 μM) was added to 1-octanol-saturated PBS, and the solutions were stirred for 30 min at room temperature in duplicate. After centrifugation, the upper layer (1-octanol) and the lower layer (PBS) were collected, and the concentrations

DMD Fast Forward. Published on October 23, 2022 as DOI: 10.1124/dmd.122.001000
This article has not been copyedited and formatted. The final version may differ from this version.
Manuscript number: DMD-AR-2022-001000

in each layer were determined by LC-MS/MS. The distribution coefficient (LogD) was calculated from the following equation:

LogD = log10 [(peak area in the 1-octanol layer) / (peak area in the PBS layer)] (34)

Metabolite Detection in PXB Cells

[^{3}H]DS-1971a (1 μM) was incubated in triplicate with PXB cells (8×10^5 cells/mL) at 37°C and 5% CO_2 for 2 h. After the reaction had been terminated by the addition of two volumes of acetonitrile, the mixture was centrifuged at 21,500g for 5 min. The resulting supernatant was analyzed by radio-HPLC.

Radio-HPLC and LC-MS/MS Analyses

Analyses were performed as previously described (Asano et al., 2021).

DMD Fast Forward. Published on October 23, 2022 as DOI: 10.1124/dmd.122.001000
This article has not been copyedited and formatted. The final version may differ from this version.
Manuscript number: DMD-AR-2022-001000

Results

Metabolite Profiling in SCID and PXB-mice

To identify DS-1971a metabolites formed in SCID and PXB-mice, plasma (at 1 h), urinary (0–24 h), and fecal (0–24 h) samples were collected after the oral administration of [^{3}H]DS-1971a (10 mg/kg), and metabolite profiling was performed. Radiochromatograms of the plasma, urinary, and fecal extracts indicated that major metabolites in SCID mice were AO-related metabolites, M4, M7, and M8, while those in PXB-mice were M1 and M2 (Fig. 3). The results indicated that the metabolite profile in PXB-mice was very similar to that in humans (Asano et al., 2022), but markedly distinct from that in SCID mice.

The PK profiles of major metabolites were then investigated to evaluate the exposure level of M1 and the AUC ratio of M1 to DS-1971a (M1/P ratio) in both types of mice. Based on the PK parameters (Supplementary Table S1), which were calculated from PK profiles (Supplementary Fig. S1), M1/P ratios in SCID and PXB-mice were determined to be 0.0 and 0.69, respectively, suggesting that the M1/P ratio in PXB-mice (0.69) was approximately half that in humans (1.6) (Table 1 and Fig. 5). In addition, dose-normalized M1 AUC in PXB-mice (1984 ng·h/mL) was approximately one-ninth that in humans (18,400 ng·h/mL) (Table 1).

Determination of Plasma PK Parameters and Fractional Metabolite Clearance in PXB-mice for PBPK Modeling

The obtained results showing that the M1/P ratio and M1 AUC in PXB-mice were much smaller than those in humans indicated that static and dynamic PBPK models were necessary for the quantitative prediction of the M1/P ratio and/or M1 AUC. Therefore, various PK parameters, including plasma V_{dss}, total, apparent oral, metabolic, renal and biliary plasma clearance, oral bioavailability, the fraction metabolized into M1 ($f_{CL,m}$), and liver-to-plasma ratio (K_{ph}) of DS-1971a and/or M1, were obtained as follows and are summarized in Supplementary Table S3 to perform PBPK modeling.

Plasma V_{dss}, total plasma clearance, apparent oral plasma clearance and oral

DMD Fast Forward. Published on October 23, 2022 as DOI: 10.1124/dmd.122.001000
This article has not been copyedited and formatted. The final version may differ from this version.
Manuscript number: DMD-AR-2022-001000

bioavailability in PXB-mice: After DS-1971a or M1 was intravenously injected into PXB-mice, plasma samples were successively collected up to 24 h and analyzed by LC-MS/MS. Using the non-compartmental method, plasma Vd_{ss} and total plasma clearance (*CL*p,total and *CL*m,total) of DS-1971a and M1 were determined to be 0.34 and 0.23 L/kg, and 20 and 11 mL/min/kg, respectively (Supplementary Table S2). After oral administration of DS-1971a, plasma concentrations of DS-1971a and M1 were quantified in the same way as for intravenous samples. The oral bioavailability of DS-1971a was calculated to be 60% in PXB-mice by dividing the oral AUC by the intravenous AUC. The apparent oral plasma clearance (*CL*/*F*) of DS-1971a and M1 were determined to be 33 and 50 mL/min/kg, respectively.

Metabolic, renal and biliary plasma clearance in PXB-mice: The urinary and fecal recovery of radioactivity in 0–24 h after the oral administration of [^{3}H]DS-1971a to PXB-mice at 10 mg/kg was determined to be 47% and 39%, respectively (Table 2). The 0–24 h recovery of DS-1971a in urine and feces was calculated to be 0.42% and 0.82%, while that of M1 was 15% and 9.2%, respectively, by multiplying the urinary and fecal recovery by the composition ratio of DS-1971a and M1 in the urinary and fecal radiochromatograms. The renal and biliary plasma clearance of DS-1971a (*CL*rp and *CL*bp) were determined to be 0.14 and 0.27 mL/min/kg, while for M1 (*CL*rm and *CL*bm) they were 7.1 and 4.6 mL/min/kg, respectively, based on eq. (2-5). The metabolic plasma clearance of DS-1971a and M1 (*CL*mp and *CL*mm) were calculated to be 20 and 0.0 mL/min/kg, respectively, by eq. (6) and (7).

f*CL*,m in PXB-mice: The urinary and fecal recovery of radioactivity during 0–72 h after the oral administration of [^{3}H]DS-1971a to PXB-mice at 10 mg/kg was determined to be 51% and 45%, respectively, indicating that most of the administered DS-1971a was excreted within 72 h (Table 2). The urinary and fecal recovery of M1 during 0–72 h was calculated to be 15% and 9.6%, respectively, by multiplying each recovery by the composition ratio of M1 in the radiochromatogram. The total recovery of M1 was calculated to be 25% up to 72 h after dosing, indicating that the fraction metabolized into M1, f*CL*,m, was 0.25.

***K*ph in PXB-mice**: Plasma and liver were collected 1 h after the oral administration

DMD Fast Forward. Published on October 23, 2022 as DOI: 10.1124/dmd.122.001000
This article has not been copyedited and formatted. The final version may differ from this version.
Manuscript number: DMD-AR-2022-001000

of [^{3}H]DS-1971a to PXB-mice at 10 mg/kg, and the radioactivity was quantified using a liquid scintillation counter and analyzed by radio-HPLC. *K*ph of DS-1971a and M1 (*K*php and *K*phm) were calculated to be 3.2 and 1.1, respectively, by dividing the liver concentrations of DS-1971a and M1 by their plasma concentrations.

Development of a PBPK Model for PXB-mice

Although the static model provides only M/P ratios but not metabolite AUC, PBPK models can estimate both of them. Before PBPK simulation for humans, we evaluated the validity of the constructed PBPK model (Fig. 2) by comparing the simulated and observed PK profiles in PXB-mice.

Detailed parameters for PBPK modeling in PXB-mice (Supplementary Table S4) were experimentally obtained, taken from the literature (Davies and Morris, 1993; Sinozuka et al., 2020; Asano et al., 2021, 2022), or calculated based on the observed PK parameters of DS-1971a and M1 (Supplementary Table S3). Using a PBPK model (Fig. 2) inputted with these PBPK parameters obtained with PXB-mice (Supplementary Table S4), the PK profiles of DS-1971a and M1 after the oral administration of DS-1971a at 10 mg/kg were simulated. As shown in Supplementary Fig. S2, the simulated PK profiles of DS-1971a and M1 in PXB-mice were relatively close to the observed ones. In addition, the simulated C_{max} and AUC values of DS-1971a and M1 were within 1.5-fold of observed data (Supplementary Table S5), and the estimated M1/P ratio was almost the same as the actual one. Thus, the PBPK model for PXB-mice was found to be established and the disposition of DS-1971a in PXB-mice was adequately expressed by the model.

Protein Binding of DS-1971a in Human Liver Microsomes and S9

The free fractions of DS-1971a in human liver microsomes and S9 (*f*u,mic and *f*u,S9) were determined to be 0.70 ± 0.06 and 0.77 ± 0.06, respectively. These values were used to calculate unbound intrinsic clearance *(*$CL_{uint,P450}$ and $CL_{uint,AO}$) in vitro.

DMD Fast Forward. Published on October 23, 2022 as DOI: 10.1124/dmd.122.001000
This article has not been copyedited and formatted. The final version may differ from this version.
Manuscript number: DMD-AR-2022-001000

Enzyme Kinetics for DS-1971a Depletion and M1 Formation in Humans for the Determination of Human f*CL*,m

One of the critical parameters for estimating metabolite exposure in the static and dynamic PBPK models in PXB-mice and humans is the fraction metabolized into M1, f*CL*,m. To obtain this value in humans, DS-1971a depletion and M1 formation were assessed using HLM. Note that intestinal DS-1971a depletion and M1 formation were ignored because no depletion or M1 formation was observed when DS-1971a was incubated with human intestinal microsomes (data not shown).

After 10-min incubation of DS-1971a in HLM with the NADPH-regenerating system at concentrations ranging from 0.1 to 30 μM, DS-1971a and M1 concentrations were quantified by LC-MS/MS. Based on the depletion and formation rates of DS-1971a and M1 at various concentrations, K_m and V_{max} values were determined to be 4.2 ± 2.8 μM and 401 ± 85 pmol/min/mg microsomal protein for DS-1971a depletion, and 4.4 ± 0.5 μM and 228 ± 6.6 pmol/min/mg microsomal protein for M1 formation, respectively (Fig. 4). Considering that $CL_{uint,P450}$ for DS-1971a depletion and M1 formation were calculated to be 137 and 73 μL/min/mg microsomal protein, respectively, and $CL_{uint,AO}$ for DS-1971a depletion was determined to be 3.8 μL/min/mg S9 protein based on the previously reported $CL_{int,AO}$ value of 2.9 μL/min/mg S9 protein (Asano et al., 2021), f*CL*,m in humans was estimated to be 0.50 (Table 3).

Membrane Permeability of DS-1971a in MDCK II Cells and Estimation of Absorption Constants-1 and -2 in Humans

Apparent permeability (P_{app}) of DS-1971a was determined to be 6.4 ± 3.8 × 10^{-6} cm/s. Based on the P_{app} value, effective permeability (P_{eff}) and absorption constants (*k*a1 and *k*a2) were calculated to be 0.80 × 10^{-4} cm/s and 0.33 /h, respectively, based on eq. (33) and (32).

DMD Fast Forward. Published on October 23, 2022 as DOI: 10.1124/dmd.122.001000
This article has not been copyedited and formatted. The final version may differ from this version.
Manuscript number: DMD-AR-2022-001000

Prediction of M1 Exposure in Humans Based on Static and PBPK Models

Since various clearance values (renal, biliary, and metabolic clearance) of DS-1971a and M1 in humans were required for both the static and dynamic PBPK models, they were estimated from those obtained with PXB-mice using the allometric scaling method (Table 4). Obtained renal, biliary, and metabolic plasma clearance were 0.0, 0.1, and 4.3 for DS-1971a and 1.6, 1.0, and 0.0 mL/min/kg for M1, respectively. These results indicated that most of the administered DS-1971a was eliminated by hepatic metabolism (i.e., metabolic clearance >> urinary and biliary clearance of DS-1971a), while M1 produced in the liver was excreted into bile and urine without further metabolism in humans (i.e., metabolic clearance of M1 = 0.0) likely due to its hydrophilicity (LogD value = –0.8), which is supported by there being no declining trend when M1 was incubated with human liver microsomes or S9 (Asano et al., 2022). Additional PBPK parameters, including intestinal availability, distribution volume, unbound fraction in plasma, liver to plasma ratio, and physiological parameters (liver blood flow and volume), were calculated, experimentally obtained, estimated, or adopted from those in PXB-mice or taken from the literature (Davies and Morris, 1993; Sinozuka et al., 2020; Asano et al., 2021, 2022), and they are summarized in Table 5.

Based on the estimated human PK parameters and f*CL*,m, the M1/P ratio in humans was calculated as 1.3 (Table 4 and Fig. 5) by the static model. This indicated that the static model gave a more accurate M1/P value than that observed in PXB-mice (0.69) since that in humans was 1.6 (Table 1 and Fig. 5).

We further tried to predict the human PK profiles of DS-1971a and M1 using the dynamic PBPK model whose important parameters (Table 5) were derived from the estimated human PBPK parameters (Table 4). Although the absorption process in actual PK profiles of DS-1971a and M1 was more sustained and delayed than that in their simulated PK profiles (Fig. 6), the C_{max} values of DS-1971a and M1 (3082 and 3429 ng/mL, respectively) in humans predicted by the PBPK modeling were similar to the observed ones (2950 and 3180 ng/mL, respectively) and the estimated AUC levels of DS-1971a and M1 (13,479 and 17,116 ng·h/mL,

DMD Fast Forward. Published on October 23, 2022 as DOI: 10.1124/dmd.122.001000
This article has not been copyedited and formatted. The final version may differ from this version.
Manuscript number: DMD-AR-2022-001000

respectively) were very close to the observed values (12,500 and 18,400 ng·h/mL, respectively) (Table 6). The M1/P ratio obtained by the dynamic PBPK model (1.3) was the same as that obtained by the static model (1.3) (Fig. 5).

Determination of LogD Values of DS-1971a, M1, M2, and M4

To consider physicochemical properties, LogD values of DS-1971a, M1, M2, and M4 at pH 7.4 were determined to be 0.8, –0.8, –0.5, and 1.5, respectively, indicating that both M1 and M2, the monooxides at the cyclohexane ring (Fig. 1), are very polar, while M4 possessing the monooxidized pyrimidine ring (Fig. 1) is more lipophilic than the intact form.

DMD Fast Forward. Published on October 23, 2022 as DOI: 10.1124/dmd.122.001000
This article has not been copyedited and formatted. The final version may differ from this version.
Manuscript number: DMD-AR-2022-001000

Discussion

In this study, we introduced a practical evaluation method to predict the exposure level of a human disproportionate metabolite of DS-1971a using PXB-mice and PBPK techniques. After the PK profiles of DS-1971a and M1 in PXB-mice were evaluated, a PBPK model for PXB-mice was developed based on the PK parameters obtained with PXB-mice to verify the model. Finally, human PK parameters were estimated from those in PXB-mice and inputted into the PBPK model for humans, leading to successful prediction of the metabolite exposure.

Drastic differences in the metabolite profiles between PXB-mice and SCID mice suggested the usefulness of PXB-mice for qualitative estimation of human major metabolites of mixed AO and P450 substrates. After the oral administration of DS-1971a, the most and second most abundant metabolites in PXB-mice were M1 and M2, respectively, both of which corresponded to those in humans produced by P450 (Asano et al., 2022), while major metabolites in SCID mice were AO-related metabolites, M4, M7, and M8 (Fig. 3, Supplementary Fig. S1, and Supplementary Table S1). The PXB-mouse was the only animal model whose metabolite profile of DS-1971a was similar to that in humans (Asano et al., 2022), considering that the predominant metabolites in male ICR mouse, monkey, rat, and dog plasma were molecules other than M1, namely, M4, M2, M5, and M11, respectively (Asano et al., 2021; and data not shown).

The PXB-mouse was also found to be a predictive animal model of human disproportionate metabolite formation by CYP2C8. Our recent work demonstrated that humans possess much higher activity for M1 formation, which is predominantly mediated by CYP2C8, than any other animals (ICR mice, rats, dogs, and monkeys) (Asano et al., 2022). Even though monkeys possess CYP2C8 [previously termed CYP2C20] with high amino acid sequence homology (92%) to human CYP2C8, much lower activity for 6α-hydroxy paclitaxel formation by CYP2C8 in monkeys than in humans is also known (Yoda et al., 2012; Emoto et al., 2013). Owing to such species-dependence in CYP2C8 metabolism, M1 exposure in humans was not covered by experiments with safety animals, leading to M1 becoming a human

DMD Fast Forward. Published on October 23, 2022 as DOI: 10.1124/dmd.122.001000
This article has not been copyedited and formatted. The final version may differ from this version.
Manuscript number: DMD-AR-2022-001000

disproportionate metabolite (Asano et al., 2022). The highest exposure to M1 of all the DS-1971a metabolites in PXB-mice (Fig. 3, Supplementary Fig. S1, and Supplementary Table S1) indicated the dominant contribution of CYP2C8 to DS-1971a metabolism in these mice. Given the additional fact that 3-hydroxydesloratadine-glucronide, which is another human disproportionate metabolite produced sequentially by UGT2B10, CYP2C8 and then UGTs (Kazumi et al., 2015), was also detected as the predominant metabolite in the plasma of PXB-mice after oral administration of desloratadine (Kato et al., 2020), PXB-mice can provide reliable qualitative information for CYP2C8-mediated formation of human disproportionate metabolites of mixed non-P450 and P450 substrates.

Meanwhile, from a quantitative perspective, the underestimation of the human M1 to DS-1971a AUC ratio (M1/P ratio) in PXB-mice deserves attention, although the M1/P ratio in PXB-mice (0.69) was closer to that in humans (1.6) than those in ICR mice (0.0), SCID mice (0.0), rats (0.16), dogs (0.0), and monkeys (0.12) (Table 1 and Fig. 5). Underestimation of the M/P ratio in PXB-mice was also observed with various compounds and their metabolites: AUC ratios of troglitazone and its sulfate, of zaleplon and its 5-oxo metabolite, and of GDC-0834 and its hydrolyzed metabolite in humanized mice were 0.5 (Schulz-Utermoehl et al., 2012), 1.7 (Tanoue et al., 2013), and 0.7 (Liu et al., 2013), respectively, and they were lower than those in humans [6.8–8.1 (Young et al., 1998), 2.9 (Smith et al., 2009), and an incalculably large value due to no exposure to the parent (Liu et al., 2013), respectively]. Though there is a possibility that innate functions of tissues other than liver (e.g., kidney) in PXB-mice might make a difference in M1/P AUC ratios between PXB-mice and humans, we found that the leading reason for the smaller M1/P AUC ratios in PXB-mice than in humans is the smaller fraction of clearance of DS-1971a for metabolite (M1) formation (f*CL*,m) in PXB-mice than in humans. In fact, the f*CL*,m in PXB-mice (0.25, Supplementary Table S4) was actually half that in humans (0.50, Table 4), probably due to metabolism by remaining mouse hepatocytes in PXB-mice (Kamimura et al., 2010). This assumption is supported by more abundant formation of M4 than M1 (Supplementary Fig. S3 (A)) and the f*CL*,m value of 0.27 (data not shown) in

DMD Fast Forward. Published on October 23, 2022 as DOI: 10.1124/dmd.122.001000
This article has not been copyedited and formatted. The final version may differ from this version.
Manuscript number: DMD-AR-2022-001000

hepatocytes from PXB-mice (PXB cells). Although there was negligible M4 in the plasma, urine, and feces from PXB-mice (Fig. 3), M4 was detected in the liver from PXB-mice (Supplementary Fig. S3 (B)), indicating that M4, which was more hydrophobic (LogD = 1.5) than the intact form and M1 (LogD = 0.8 and −0.8), was likely metabolized into further metabolites including M8 and M9 due to its poor metabolic stability (Asano et al., 2022). The slight difference of M1/P ratios between PXB-mice (0.69) and humans (1.6) directed us to the additional research on estimation of the human M1/P ratio by static and dynamic PBPK methods.

Prior to the estimation of the M1/P ratio in humans, a robust PBPK model for PXB-mice (Fig. 2) was constructed. In this research, we focused on the PK parameters of C_{max} and AUC because these parameters are used as criteria for disproportionate metabolite and safety assessment in the US Food and Drug Administration (FDA) guidance for industry on safety testing of drug metabolites (FDA, 2020) and/or ICH guidance (International Conference on Harmonisation [ICH], 2010). Since the simulated C_{max}, AUC, and M1/P ratios in PXB-mice were close to the observed values (Supplementary Table S5), we moved forward with human PK prediction.

The human PBPK model was developed based on the same model structure (Fig. 2) as that for PXB-mice with the replacement of parameters in PXB-mice by those in humans, enabling the prediction of exposure to DS-1971a and M1 in humans. Important PK parameters in humans such as V_{dss} and various clearance (Table 4) were estimated by the allometric scaling of PK parameters in PXB-mice as the only animal model showing as high exposure to M1 as humans (Fig. 3). The human PBPK model, in which various parameters (Table 5) converted from those in Table 4 were inputted, successfully provided us with C_{max} and AUC (3082 ng/mL and 3429 ng/mL, and 13,479 and 17,116 ng·h/mL) of DS-1971a and M1, which were very close to the observed values (2950 and 3180 ng/mL, and 12,500 and 18,400 ng·h/mL) (Table 6). Meanwhile, the simulated PK profile lacked the prolonged absorption profile of the actual one (Fig. 6.). A potential reason for this is the delayed absorption in the fed condition because enterohepatic circulation of DS-1971a was not observed in mice and

DMD Fast Forward. Published on October 23, 2022 as DOI: 10.1124/dmd.122.001000
This article has not been copyedited and formatted. The final version may differ from this version.
Manuscript number: DMD-AR-2022-001000

monkeys (Asano et al., 2021), and DS-1971a was administered to humans after ingestion of high-calorie food. Food has strong influence on absorption process of drugs based on previous research reporting that gastric transit time was prolonged up to 5 h by the presence of food in the gastrointestinal tract (Weitschies et al., 2010). The lack of adequate simulation of the absorption process under fed conditions is a limitation of this research, as illustrated by the better simulated PK results using optimized absorption and transit constants (Supplementary Fig. S4). Another limitation was the lack of inclusion of transporters (TPs) in the model. Although we quantified various clearance based on PK results, the contribution of TPs to these parameters was not estimated.

Both static and dynamic models provided us with the same M1/P ratio (1.3), which is close to the observed value (1.6). Although the static model appears to be more useful due to the smaller number of PK parameters required for the calculation, the accuracy of the parameters should be examined using a dynamic model. For example, the plasma C_{max} and AUC of DS-1971a and M1 simulated by the dynamic model were comparable to those observed (Supplementary Fig. S2 and Supplementary Table S5), thereby confirming the validity of the obtained parameters, such as hepatic and systemic clearance, which are also used to perform static calculation. Therefore, it is better to use both static and dynamic models in combination to reproduce the observed data and which method is selected would depend on a case-by-case basis. Although the construction of a dynamic model requires numerous parameters, a dynamic model has a wide range of applications, such as in drug–drug interaction (DDI) simulation (Yamada et al., 2020), pharmacokinetics-pharmacodynamics (PK/PD) (Loisios-Konstantinidis et al., 2020), and model-informed drug discovery and development (MID3) (Marshall et al., 2016).

In conclusion, we have demonstrated that PXB-mice are useful to predict the PK of and exposure to human disproportionate metabolites generated by CYP2C8-mediated primary metabolism. Although the metabolite profiles of DS-1971a and M1 in PXB-mice were very similar to those in humans, the observed M1/P ratio in PXB-mice underestimated that in

DMD Fast Forward. Published on October 23, 2022 as DOI: 10.1124/dmd.122.001000
This article has not been copyedited and formatted. The final version may differ from this version.

humans. The present results suggest that PBPK modeling based on not only estimated human PK parameters obtained with PXB-mice but also metabolite formation kinetics in human liver fractions is a practical method to predict the human PK profile of M1 and its exposure level in a quantitative manner.

Manuscript number: DMD-AR-2022-001000

Acknowledgments

The authors thank PhoenixBio for their generous support.

Author Contributions

Participated in research design: Asano

Conducted experiments: Asano, Hamada

Performed data analysis: Asano, Nakamura, Nishiya, Yahara

Wrote or contributed to the writing of the manuscript: Asano, Nakamura, Nishiya, Shiozawa, Takakusa, Shibayama, Inoue, Shinozuka, Yahara, Watanabe, Yoshinari

DMD Fast Forward. Published on October 23, 2022 as DOI: 10.1124/dmd.122.001000
This article has not been copyedited and formatted. The final version may differ from this version.
Manuscript number: DMD-AR-2022-001000

References

Asano D, Hamaue S, Zahir H, Shiozawa H, Nishiya Y, Kimura T, Kazui M, Yamamura N, Ikeguchi M, Shibayama T, Inoue SI, Shinozuka T, Watanabe T, Yahara C, Watanabe N and Yoshinari K (2022) CYP2C8-mediated formation of a human disproportionate metabolite of the selective $Na_V1.7$ inhibitor DS-1971a, a mixed cytochrome P450 and aldehyde oxidase substrate. *Drug Metab Dispos* **50**: 235-242.

Asano D, Shibayama T, Shiozawa H, Inoue SI, Shinozuka T, Murata S, Watanabe N, and Yoshinari K (2021) Evaluation of species differences in the metabolism of the selective NaV1.7 inhibitor DS-1971a, a mixed substrate of cytochrome P450 and aldehyde oxidase. *Xenobiotica* **51**: 1060-1070.

Callegari E, Varma MVS, and Obach RS (2020) Prediction of metabolite-to-parent drug exposure: Derivation and application of a mechanistic static model. *Clin Transl Sci* **13**: 520-528.

Davies B and Morris T (1993) Physiological parameters in laboratory animals and humans. *Pharm Res* **10**: 1093-1095.

Emoto C, Yoda N, Uno Y, Iwasaki K, Umehara K, Kashiyama E, and Yamazaki H (2013) Comparison of p450 enzymes between cynomolgus monkeys and humans: p450 identities, protein contents, kinetic parameters, and potential for inhibitory profiles. *Curr Drug Metab* **14**: 239-252.

Food and Drug Administration (FDA) (2020) Guidance for Industry: Safety Testing of Drug Metabolites. Center for Drug Evaluation and Research, U.S. *Food and Drug Administration, U.S. Department of Health and Human Services*, Silver Spring, MD.

Furukawa A, Schwochert J, Pye CR, Asano D, Edmondson QD, Turmon AC, Klein VG, Ono S, Okada O, and Lokey RS (2020) Drug-like properties in macrocycles above MW 1000: Backbone rigidity versus side-chain lipophilicity. *Angew Chem Int Ed Engl* **59**: 21571-21577.

Gill KL, Gertz M, Houston JB, and Galetin A (2013) Application of a physiologically based pharmacokinetic model to assess propofol hepatic and renal glucuronidation in isolation: Utility of in vitro and in vivo data. *Drug Metab Dispos* **41**: 744-753.

Hasegawa M, Tahara H, Inoue R, Kakuni M, Tateno C, and Ushiki J (2012) Investigation of drug-drug interactions caused by human pregnane X receptor-mediated induction of CYP3A4

and CYP2C subfamilies in chimeric mice with a humanized liver. *Drug Metab Dispos* **40**: 474-480.

International Conference on Harmonisation (ICH) (2010) M3(R2) Guidance: Nonclinical Safety Studies for the Conduct of Human Clinical Trials and Marketing Authorization for Pharmaceuticals. *ICH*, Geneva, Switzerland.

Houston JB and Galetin A (2008) Methods for predicting in vivo pharmacokinetics using data from in vitro assays. *Curr Drug Metab* **9**: 940-951.

Ito S, Kamimura H, Yamamoto Y, Chijiwa H, Okuzono T, Suemizu H, and Yamazaki H (2020) Human plasma concentration-time profiles of troglitazone and troglitazone sulfate simulated by in vivo experiments with chimeric mice with humanized livers and semi-physiological pharmacokinetic modeling. *Drug Metab Pharmacokinet* **35**: 505-514.

Kamimura H, Nakada N, Suzuki K, Mera A, Souda K, Murakami Y, Tanaka K, Iwatsubo T, Kawamura A, and Usui T (2010) Assessment of chimeric mice with humanized liver as a tool for predicting circulating human metabolites. *Drug Metab Pharmacokinet* **25**: 223-235.

Kato S, Shah A, Plesescu M, Miyata Y, Bolleddula J, Chowdhury S, and Zhu X (2020) Prediction of human disproportionate and biliary excreted metabolites using chimeric mice with humanized liver. *Drug Metab Dispos* **48**: 934-943.

Kazmi F, Barbara JE, Yerino P, and Parkinson A (2015) A long-standing mystery solved: the formation of 3-hydroxydesloratadine is catalyzed by CYP2C8 but prior glucuronidation of desloratadine by UDP-glucuronosyltransferase 2B10 is an obligatory requirement. *Drug Metab Dispos* **43**:523-533.

Kenyon C, Hooper G, Tierney D, Butler J, Devane J, and Wilding I (1995) The effect of food on the gastrointestinal transit and systemic absorption of naproxen from a novel sustained release formulation, *J Control Release* **34**: 31-36.

Liu L, Halladay JS, Shin Y, Wong S, Coraggio M, La H, Baumgardner M, Le H, Gopaul S, Boggs J, Kuebler P, Davis JC, Jr., Liao XC, Lubach JW, Deese A, Sowell CG, Currie KS, Young WB, Khojasteh SC, Hop CE and Wong H (2011) Significant species difference in amide hydrolysis of GDC-0834, a novel potent and selective Bruton's tyrosine kinase inhibitor. *Drug Metab Dispos* **39**: 1840-1849.

Loisios-Konstantinidis I, Cristofoletti R, Jamei M, Turner D, and Dressman J (2020) Physiologically based pharmacokinetic/pharmacodynamic modeling to predict the impact of CYP2C9 genetic polymorphisms, co-medication and formulation on the pharmacokinetics and pharmacodynamics of flurbiprofen. *Pharmaceutics* **12**: 1049.

Marshall SF, Burghaus R, Cosson V, Cheung SY, Chenel M, DellaPasqua O, Frey N, Hamren B, Harnisch L, Ivanow F, Kerbusch T, Lippert J, Milligan PA, Rohou S, Staab A, Steimer JL, Tornoe C, and Visser SA (2016) Good practices in model-informed drug discovery and development: Practice, application, and documentation. *CPT Pharmacometrics Syst Pharmacol* **5**: 93-122.

Nagata T, Yoshino T, Haginoya N, Yoshikawa K, Nagamochi M, Kobayashi S, Komoriya S, Yokomizo A, Muto R, Yamaguchi M, Osanai K, Suzuki M, and Kanno H (2009) Discovery of N-[(1R,2S,5S)-2-{[(5-chloroindol-2-yl)carbonyl]amino}-5-(dimethylcarbamoyl)cycloh exyl]-5-methyl-4,5,6,7-tetrahydrothiazolo[5,4-c]pyridine-2-carboxamide hydrochloride: a novel, potent and orally active direct inhibitor of factor Xa. *Bioorg Med Chem* **17**: 1193-1206.

Nguyen HQ, Kimoto E, Callegari E, and Obach RS (2016) Mechanistic modeling to predict midazolam metabolite exposure from in vitro data. *Drug Metab Dispos* **44**: 781-791.

Obach RS, Baxter JG, Liston TE, Silber BM, Jones BC, MacIntyre F, Rance DJ, and Wastall P (1997) The prediction of human pharmacokinetic parameters from preclinical and in vitro metabolism data. *J Pharmacol Exp Ther* **283**: 46-58.

Obach RS, Lin J, Kimoto E, Duvvuri S, Nicholas T, Kadar EP, Tremaine LM, and Sawant-Basak A (2018) Estimation of circulating drug metabolite exposure in human using in vitro data and physiologically based pharmacokinetic modeling: Example of a high metabolite/parent drug ratio. *Drug Metab Dispos* **46**: 89-99.

Okumura H, Katoh M, Sawada T, Nakajima M, Soeno Y, Yabuuchi H, Ikeda T, Tateno C, Yoshizato K, and Yokoi T (2007) Humanization of excretory pathway in chimeric mice with humanized liver. *Toxicol Sci* **97**: 533-538.

Pleiss U (2005) [Radioactive-labeled pharmaceutical agents]. *Pharm Unserer Zeit* **34**: 514-519.

Sanoh S, Horiguchi A, Sugihara K, Kotake Y, Tayama Y, Uramaru N, Ohshita H, Tateno C, Horie T, Kitamura S and Ohta S (2012) Predictability of metabolism of ibuprofen and naproxen using

DMD Fast Forward. Published on October 23, 2022 as DOI: 10.1124/dmd.122.001000
This article has not been copyedited and formatted. The final version may differ from this version.
Manuscript number: DMD-AR-2022-001000

chimeric mice with human hepatocytes. *Drug Metab Dispos* **40**: 2267-2272.

Sanoh S, Naritomi Y, Fujimoto M, Sato K, Kawamura A, Horiguchi A, Sugihara K, Kotake Y, Ohshita H, Tateno C, Horie T, Kitamura S and Ohta S (2015) Predictability of plasma concentration-time curves in humans using single-species allometric scaling of chimeric mice with humanized liver. *Xenobiotica* **45**: 605-614.

Schulz-Utermoehl T, Sarda S, Foster JR, Jacobsen M, Kenna JG, Morikawa Y, Salmu J, Gross G, and Wilson ID (2012) Evaluation of the pharmacokinetics, biotransformation and hepatic transporter effects of troglitazone in mice with humanized livers. *Xenobiotica* **42**: 503-517.

Shinozuka T, Kobayashi H, Suzuki S, Tanaka K, Karanjule N, Hayashi N, Tsuda T, Tokumaru E, Inoue M, Ueda K, Kimoto H, Domon Y, Takahashi S, Kubota K, Yokoyama T, Shimizugawa A, Koishi R, Fujiwara C, Asano D, Sakakura T, Takasuna K, Abe Y, Watanabe T and Kitano Y (2020) Discovery of DS-1971a, a potent, selective NaV1.7 inhibitor. *J Med Chem* **63**: 10204-10220.

Smith DA and Obach RS (2009) Metabolites in safety testing (MIST): Considerations of mechanisms of toxicity with dose, abundance, and duration of treatment. *Chem Res Toxicol* **22**: 267-279.

Tang H, Hussain A, Leal M, Mayersohn M, and Fluhler E (2007) Interspecies prediction of human drug clearance based on scaling data from one or two animal species. *Drug Metab Dispos* **35**: 1886-1893.

Tanoue C, Sugihara K, Uramaru N, Tayama Y, Watanabe Y, Horie T, Ohta S, and Kitamura S (2013) Prediction of human metabolism of the sedative-hypnotic zaleplon using chimeric mice transplanted with human hepatocytes. *Xenobiotica* **43**: 956-962.

Tateno C, Miya F, Wake K, Kataoka M, Ishida Y, Yamasaki C, Yanagi A, Kakuni M, Wisse E, Verheyen F, Inoue K, Sato K, Kudo A, Arii S, Itamoto T, Asahara T, Tsunoda T and Yoshizato K (2013) Morphological and microarray analyses of human hepatocytes from xenogeneic host livers. *Lab Invest* **93**: 54-71.

Tchaparian E, Tang L, Xu G, Huang T and Jin L (2008) Cell based experimental models as tools for the prediction of human intestinal absorption: Correlation with oral drug absorption and jejunal permeability in humans. *Drug Metab Rev* **40** (Suppl. 3): 178.

Weitschies W, Blume H, and Monnikes H (2010) Magnetic marker monitoring: high resolution real-time tracking of oral solid dosage forms in the gastrointestinal tract. *Eur J Pharm Biopharm* **74**: 93-101.

Yamada M, Ishizuka T, Inoue SI, Rozehnal V, Fischer T, and Sugiyama D. (2020). Drug-drug interaction risk assessment of esaxerenone as a perpetrator by in vitro studies and static and physiologically based pharmacokinetic models. *Drug Metab Dispos* **48**: 769-777.

Yang X, Gandhi YA, Duignan DB, and Morris ME (2009) Prediction of biliary excretion in rats and humans using molecular weight and quantitative structure-pharmacokinetic relationships. *AAPS J* **11**: 511-525.

Yoda N, Emoto C, Date S, Kondo S, Miyake M, Nakazato S, Umehara K, and Kashiyama E (2012) Characterization of intestinal and hepatic P450 enzymes in cynomolgus monkeys with typical substrates and inhibitors for human P450 enzymes. *Xenobiotica* **42**: 719-730.

Young MA, Lettis S, and Eastmond R (1998) Improvement in the gastrointestinal absorption of troglitazone when taken with, or shortly after, food. *Br J Clin Pharmacol* **45**: 31-35.

Yu LX and Amidon GL (1998) Characterization of small intestinal transit time distribution in humans. *Int J Pharm* **171**: 157-163.

Yu LX and Amidon GL (1999) A compartmental absorption and transit model for estimating oral drug absorption. *Int J Pharm* **186**: 119-125.

Zhou SF, Tingle MD, Kestell P, and Paxton JW (2002) Species differences in the metabolism of the antitumour agent 5,6-dimethylxanthenone-4-acetic acid in vitro: Implications for prediction of metabolic interactions in vivo. *Xenobiotica* **32**: 87-107.

DMD Fast Forward. Published on October 23, 2022 as DOI: 10.1124/dmd.122.001000
This article has not been copyedited and formatted. The final version may differ from this version.
Manuscript number: DMD-AR-2022-001000

Footnotes

Financial disclosure: No author has an actual or perceived conflict of interest with the contents of this article. The authors are employees of Daiichi Sankyo Co., Ltd or University of Shizuoka.

Funding information: All research was funded by Daiichi Sankyo Co., Ltd with no external funding.

DMD Fast Forward. Published on October 23, 2022 as DOI: 10.1124/dmd.122.001000
This article has not been copyedited and formatted. The final version may differ from this version.

Manuscript number: DMD-AR-2022-001000

Figure legends

Fig. 1. The proposed metabolic pathway of DS-1971a from nonclinical studies.

The map was prepared based on our previous report (Asano et al., 2021). Solid and dashed arrows indicate the metabolic pathways with high and low possibility, respectively.

Fig. 2. The structure of the PBPK model of DS-1971 and M1 for PXB-mice and humans.

Ag1, drug amount in the upper intestine; Ag2, drug amount in the lower intestine; blood-*CL*rm, renal blood clearance of M1; blood-*CL*rp, renal blood clearance of DS-1971a; Cbm, blood concentration of M1; Cbp, blood concentration of DS-1971a; Chm, hepatic concentration of M1; Chp, hepatic concentration of DS-1971a; CL_{int},bm, biliary blood intrinsic clearance of M1; CL_{int},bp, biliary blood intrinsic clearance of DS-1971a; CL_{int},mp, metabolic blood intrinsic clearance of DS-1971a; f*CL*,m, fraction of the clearance of DS-1971a that yields M1; *k*a1, absorption constant-1; *k*a2, absorption constant-2; *K*phm, liver to plasma ratio of M1; *K*php, liver to plasma ratio of DS-1971a; *k*t, transit constant; *Q*h, liver blood flow; *V*h, liver volume; *V*1m, blood-based extrahepatic distribution volume of M1; *V*1p, blood-based extrahepatic distribution volume of DS-1971a;

Fig. 3. Radiochromatograms of the plasma, urine, and feces from SCID mice and

DMD Fast Forward. Published on October 23, 2022 as DOI: 10.1124/dmd.122.001000
This article has not been copyedited and formatted. The final version may differ from this version.

Manuscript number: DMD-AR-2022-001000

PXB-mice after oral dosing of radiolabeled DS-1971a at 10 mg/kg in the fasted condition.

Plasma (A, D), urine (B, E), and feces (C, F) were obtained from SCID mice (A–C) and PXB-mice (D–F) at 1 h, 0–24 h, and 0–24 h, respectively, after [^{3}H]DS-1971a administration and were analyzed using radio-HPLC. The radioactive peaks of the parent and metabolites were identified by comparing their retention times with those of authentic standards for the parent and each metabolite. * indicates unknown metabolites.

Fig. 4. K_m and V_{max} values for DS-1971a depletion and M1 formation in HLM.

DS-1971a was incubated in HLM (0.5 mg/mL) with the NADPH-regenerating system at concentrations ranging from 0.1 to 30 μM, and DS-1971a and M1 concentrations were determined after 10 minutes incubation. The rates of DS-1971a depletion (A) and M1 formation (B) were calculated based on the plots. Each plot represents the mean velocity ± SD of three incubations. Using WinNonlin 6.3, K_m and V_{max} values were determined by fitting to the simple E_{max} model (model 101) [$E = E_{max} \times C \div (EC_{50} + C)$] (eq. (12)), where E, C, E_{max}, and EC_{50} represent metabolic reaction velocity, DS-1971a concentration, V_{max}, and K_m as per the Michaelis–Menten equation, respectively.

Fig. 5. Observed and predicted plasma AUC ratios of M1 to DS-1971a in various species.

a, c: M1/P ratios (mean ± SD of n = 3[a] or 6[c]) are cited and modified from Asano et al. (2021, 2022). b: Data represent the mean ± SD (n = 3). Static model-based prediction was performed according to eq. (13). PBPK model-based estimation was performed by dividing the predicted M1 AUC by the predicted DS-1971a AUC.

Fig. 6. The predicted plasma PK profiles of DS-1971a (A) and M1 (B) in humans after oral administration at 400 mg in the fed condition using the dynamic PBPK model.

PBPK modeling was performed based on the customized model (Fig. 2) with the parameters shown in Table 5 using WinNonlin 6.3. Open and closed circles represent the observed plasma concentrations of DS-1971a and M1 (mean ± SD of six humans), respectively (Asano et al., 2022). Solid line indicates the simulated PK profiles of DS-1971a and M1 by the dynamic PBPK model.

DMD Fast Forward. Published on October 23, 2022 as DOI: 10.1124/dmd.122.001000
This article has not been copyedited and formatted. The final version may differ from this version.

Manuscript number: DMD-AR-2022-001000

Table 1. Observed plasma M1/P ratios in experimental animals and humans.

Species	Dose	DS-1971a plasma AUC (ng·h/mL)	M1 plasma AUC (ng·h/mL)	M1 dose-normalized plasma AUC[d] (ng·h/mL)	Plasma M1/P ratio
ICR mice[a]	10 mg/kg	395 ± 148	1.7 ± 0.12	0.97 ± 0.11	0.0 ± 0.0
SCID mice[b]		1736 ± 191	5.7 ± 1.6	3.3 ± 0.91	0.0 ± 0.0
PXB-mice[b]		5113 ± 548	3472 ± 253	1984 ± 145	0.69 ± 0.10
Rats[a]		3234 ± 1447	478 ± 136	273 ± 78	0.16 ± 0.038
Dogs[a]		42,949 ± 17,096	0.0 ± 0.0	0.0 ± 0.0	0.0 ± 0.0
Monkeys[a]	3 mg/kg	2485 ± 473	288 ± 20	165 ± 11	0.12 ± 0.029
Humans[c]	400 mg	12,500 ± 3700	18,400 ± 3790	-	1.6 ± 0.55

a, c: PK parameters (mean ± SD, n = 3[a] or 6[c]) are cited from Asano et al. (2021, 2022) and modified. b: Data represent the mean ± SD of three mice. d: eq. (1)

DMD Fast Forward. Published on October 23, 2022 as DOI: 10.1124/dmd.122.001000
This article has not been copyedited and formatted. The final version may differ from this version.

Manuscript number: DMD-AR-2022-001000

Table 2. The recovery of the radioactivity in urine and feces of SCID mice and PXB-mice after oral administration of [^{3}H]DS-1971a at 10 mg/kg in the fasted condition.

Excretion pathway	Cumulative radioactivity excretion (% of dose)			
	SCID mice		PXB-mice	
	0–24 h	0–72 h	0–24 h	0–72 h
Urine	1.6 ± 1.5	2.6 ± 1.3	47 ± 6.7	51 ± 5.9
Feces	87 ± 11	91 ± 8.2	39 ± 2.0	45 ± 0.51
Total (urine + feces)	88 ± 9.5	93 ± 7.0	86 ± 6.9	96 ± 5.7

Urine and feces were collected up to 72 h after oral administration of [^{3}H]DS-1971a (10 mg/kg). Each value represents the mean ± SD of three mice.

Table 3. Calculation of f*CL*,m in humans.

Evaluation items	Parameter	Human liver fraction	
		Microsomes	S9
DS-1971a depletion	$CL_{uint,P450}$ (μL/min/mg protein)	137	NA
	$CL_{uint,AO}$ (μL/min/mg protein)	NA	3.8
M1 formation	$CL_{uint,P450}$ (μL/min/mg protein)	73	NA
-	Protein abundance (mg protein/g liver)	46	121
The fraction of clearance of DS-1971a for M1 formation	f*CL*,m[a] (ratio)	0.50[a]	

$CL_{uint,P450}$ values were obtained by dividing the mean of V_{max} values by the mean of K_m values and *f*u,mic obtained from three incubations. $CL_{uint,AO}$ was calculated by dividing $CL_{int,AO}$, which is cited from Asano et al. (2021), by *f*u,S9. Protein abundance are cited from Zhou et al. (2002), and Houston and Galetin (2008). a: f*CL*,m was calculated based on eq. (14).

NA, not applicable.

Table 4. Estimation of PBPK parameters in humans using the allometric scaling method and M1/P ratio calculation based on the static model.

Parameters		DS-1971a	M1	Source	Static model	PBPK model
Molecular weight		465	481	-	X	X
Plasma distribution volume at steady state: Vd_{ss}[a] (L/kg)		0.15[a]	0.10[a]	Allometry[a]		
Detail	Blood-based extrahepatic distribution volume: $V1p$[b] or $V1m$[b] (L)	13[b]	9.8[b]	Calculated[b]		X
	Liver volume: Vh (L)	1.7		Reported (Davies and Morris, 1993)		X
	Liver to plasma ratio: Kp	3.2	1.1	Measured		X
fCL,m (ratio)		0.50	-	Calculated (Table 3)	X	X
Total plasma clearance: [c]CLp,total or [c]CLm,total (mL/min/kg)		4.4[c]	2.6[c]	Allometry[c]	X	
Detail	Metabolic plasma clearance: CLmp[c] or CLmm[c] (mL/min/kg)	4.3[c]	0.0[c]		X	X
	Biliary plasma clearance: CLbp[c] or CLbm[c] (mL/min/kg)	0.059[c]	1.0[c]		X	X
	Renal plasma clearance: CLrp[c] or CLrm[c] (mL/min/kg)	0.030[c]	1.6[c]			X
Hepatic availability: Fh,p[d] or Fh,m[e]		0.62[d]	0.92[e]	Calculated[d, e]	X	
Plasma M1/P ratio[f] by static model		1.3[f]		Calculated[f]	X	

X: used

a: eq. (9), b: eq. (31), c: eq. (8), d: eq. (10), e: eq. (11), f: eq. (13)

Table 5. Inputted parameters in the PBPK model for humans.

Inputted parameter	Explanation	Value	Unit	Source
Dose	Clinical dose	400	mg	Reported (Asano et al., 2022)
*F*a	Fraction absorbed	1.0		Reported (Asano et al., 2021)
*F*g	Intestinal availability	1.0		Calculated
Tlag	Residence time in the stomach in a fed condition	1.3	h	Reported (Kenyon et al., 1995)
Ag1	Drug amount in upper intestine	Variable	mg	-
Ag2	Drug amount in lower intestine	Variable	mg	
*V*h	Liver volume	1.7	L	Reported (Davies and Morris, 1993)
*Q*h	Liver blood flow	21	mL/min/kg	
*k*a1[a]	Absorption constant in upper intestine	0.33[a]	/h	Calculated[a]
*k*a2[a]	Absorption constant in lower intestine	0.33[a]	/h	Calculated[a]
*k*t[b]	Transit constant in gastrointestinal tract	0.57[b]	/h	Calculated[b]
MWp and MWm	Molecular weight	465, 481	g/mole	Calculated
*R*bp and *R*bm	Blood-to-plasma concentration ratio of DS-1971a and M1	0.55, 0.56	-	Measured
*f*up and *f*um	Unbound fraction of DS-1971a and M1 in plasma	0.010, 0.020	-	Reported (Shinozuka et al., 2020; Asano et al., 2022)
Chp and Chm	Hepatic concentration of DS-1971a and M1	Variable	ng/mL	-
*K*php and *K*phm	Liver-to-plasma ratio of DS-1971a and M1	3.2, 1.1	-	Measured
Cbp and Cbm	Blood concentration of DS-1971a and M1	Variable	ng/mL	-
*V*1p and *V*1m	Blood-based extrahepatic distribution volume of DS-1971a and M1	13, 9.8	L	Calculated (Table 4)
CL_{int},bp[c] and CL_{int},bm[d]	Biliary blood intrinsic clearance of DS-1971a and M1	25[c], 229[d]	L/h	Calculated[c, d]
blood-*CL*rp[e] and -*CL*rm[f]	Renal blood clearance of DS-1971a and M1	0.23[e], 12[f]	L/h	Calculated[e, f]
f*CL*,m	Fraction of the clearance of DS-1971a that yields M1	0.50	-	Calculated (Table 3)
CL_{int},mp[g]	Metabolic blood intrinsic clearance of DS-1971a	2923[g]	L/h	Calculated[g]

a: eq. (32), b. eq. (30), c: eq. (26), d: eq. (25), e: eq. (23), f: eq. (24), g: eq. (27)

DMD Fast Forward. Published on October 23, 2022 as DOI: 10.1124/dmd.122.001000
This article has not been copyedited and formatted. The final version may differ from this version.

Manuscript number: DMD-AR-2022-001000

Table 6. Observed and PBPK model-predicted plasma PK parameters for humans after 400 mg oral dose of DS-1971a in the fed condition.

Compound	Method	Plasma C_{max} (ng/mL)	Plasma AUC (ng·h/mL)	Plasma M1/P ratio
DS-1971a	Dynamic PBPK simulation	3082	13,479	-
	Observed[a]	2950 ± 1810[a]	12,500 ± 3700[a]	-
M1	Dynamic PBPK simulation	3429	17,116	1.3
	Observed[a]	3180 ± 465[a]	18,400 ± 3790[a]	1.6 ± 0.55[a]

a: PK parameters (mean ± SD of n = 6) are cited and modified from Asano et al. (2022)

DMD Fast Forward. Published on October 23, 2022 as DOI: 10.1124/dmd.122.001000
This article has not been copyedited and formatted. The final version may differ from this version.

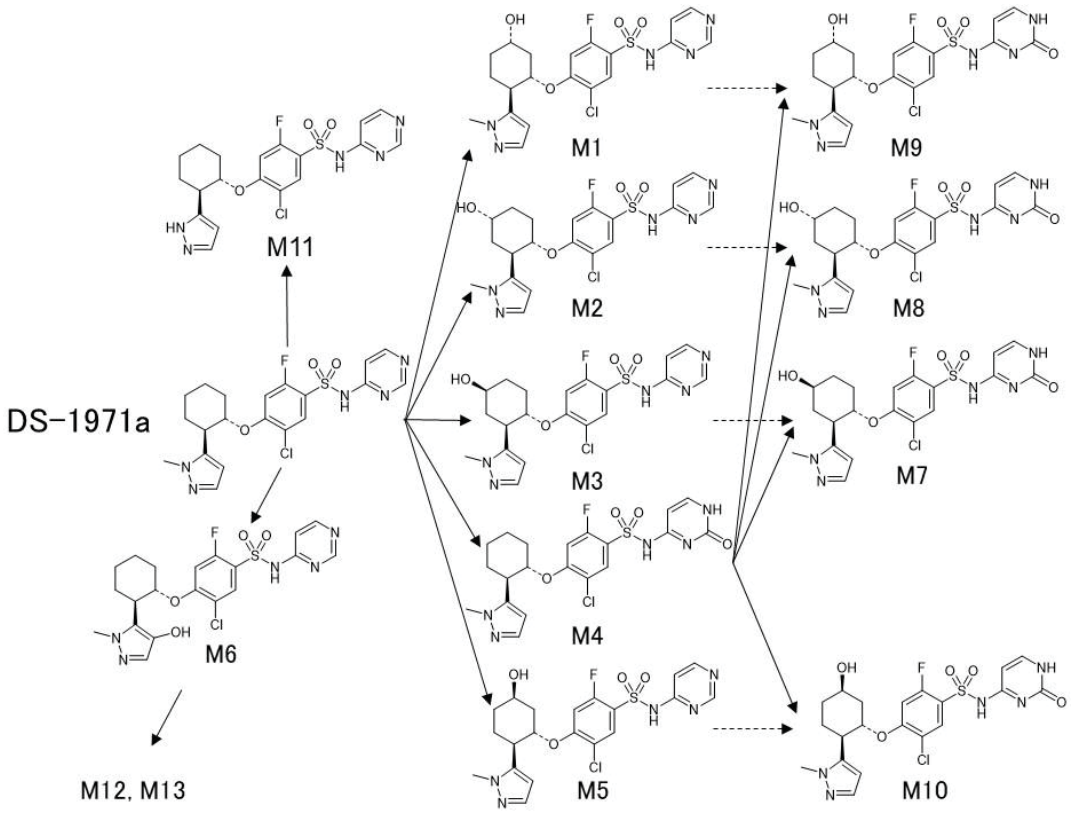

Fig. 1.

DMD Fast Forward. Published on October 23, 2022 as DOI: 10.1124/dmd.122.001000
This article has not been copyedited and formatted. The final version may differ from this version.

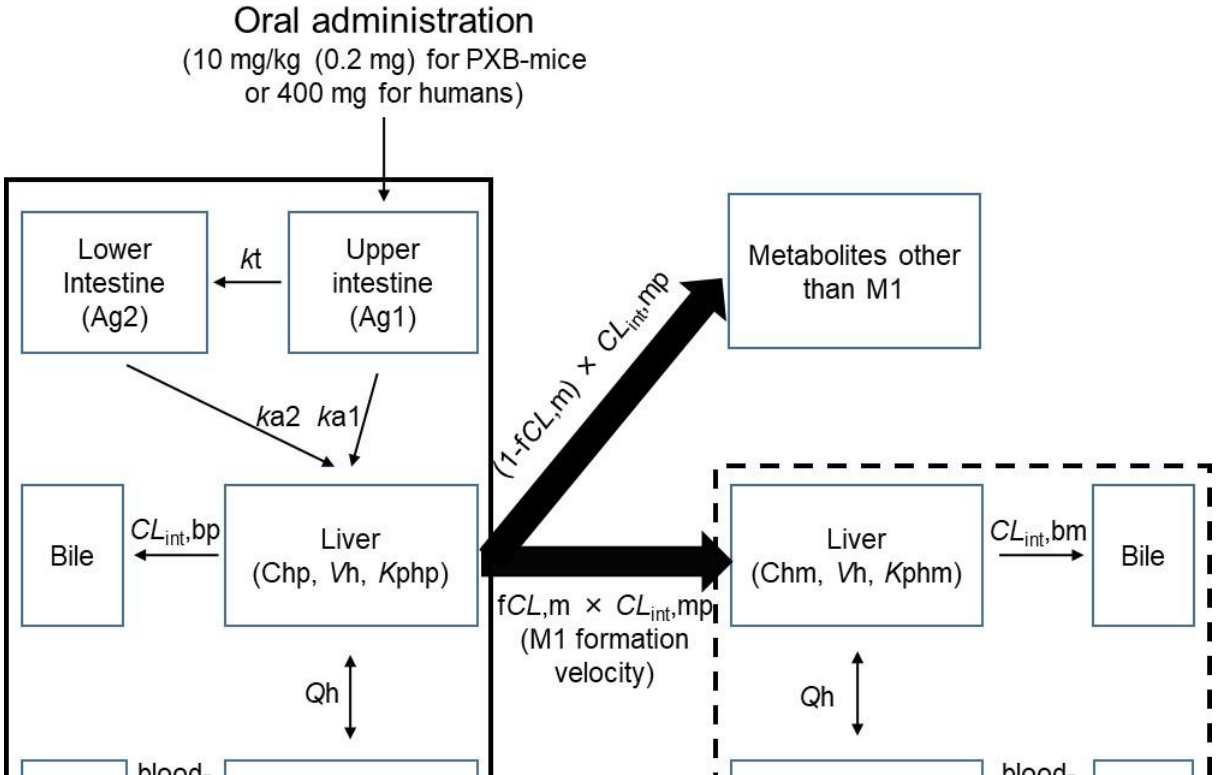

Fig. 2.

DMD Fast Forward. Published on October 23, 2022 as DOI: 10.1124/dmd.122.001000
This article has not been copyedited and formatted. The final version may differ from this version.

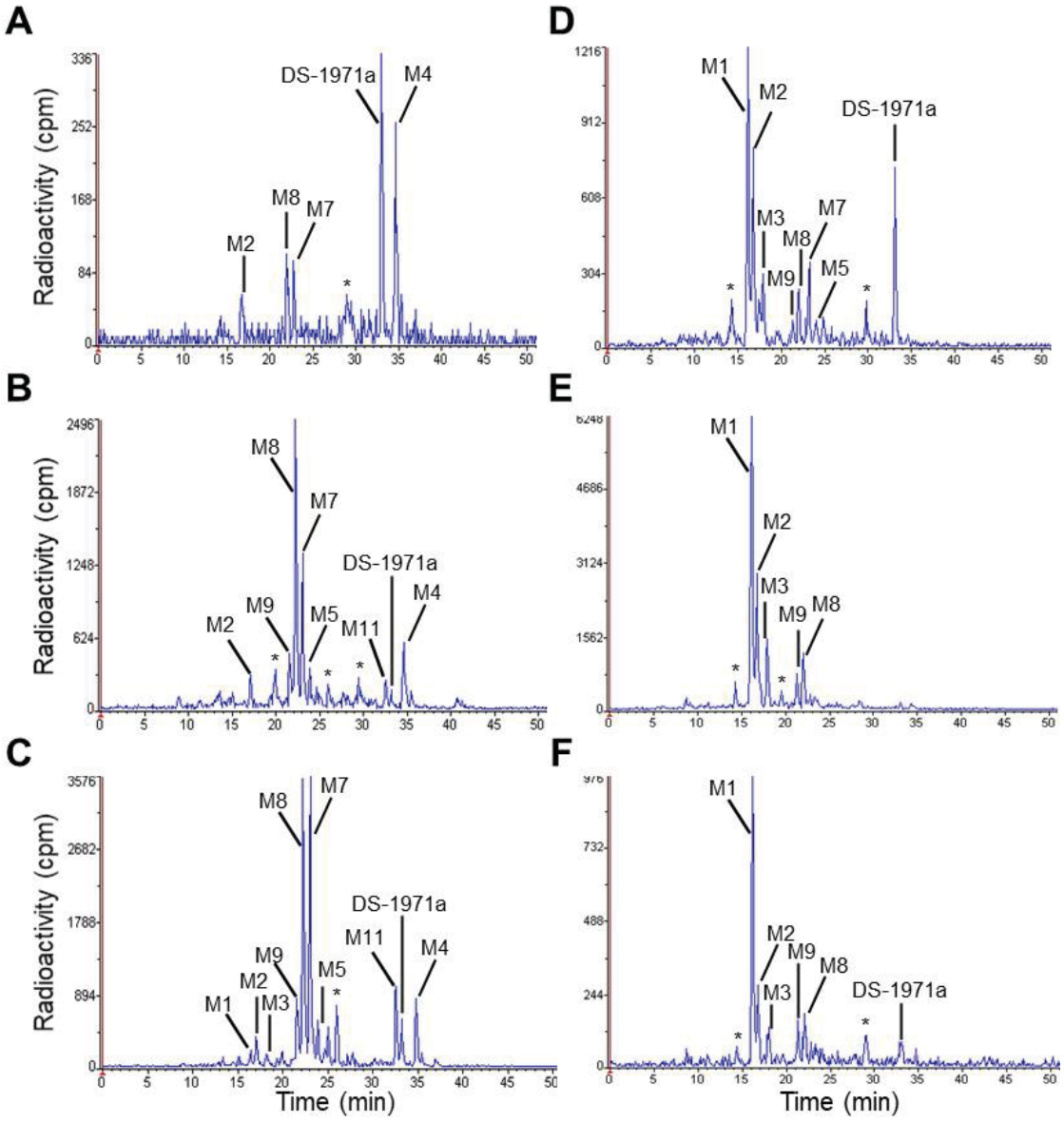

Fig. 3.

DMD Fast Forward. Published on October 23, 2022 as DOI: 10.1124/dmd.122.001000
This article has not been copyedited and formatted. The final version may differ from this version.

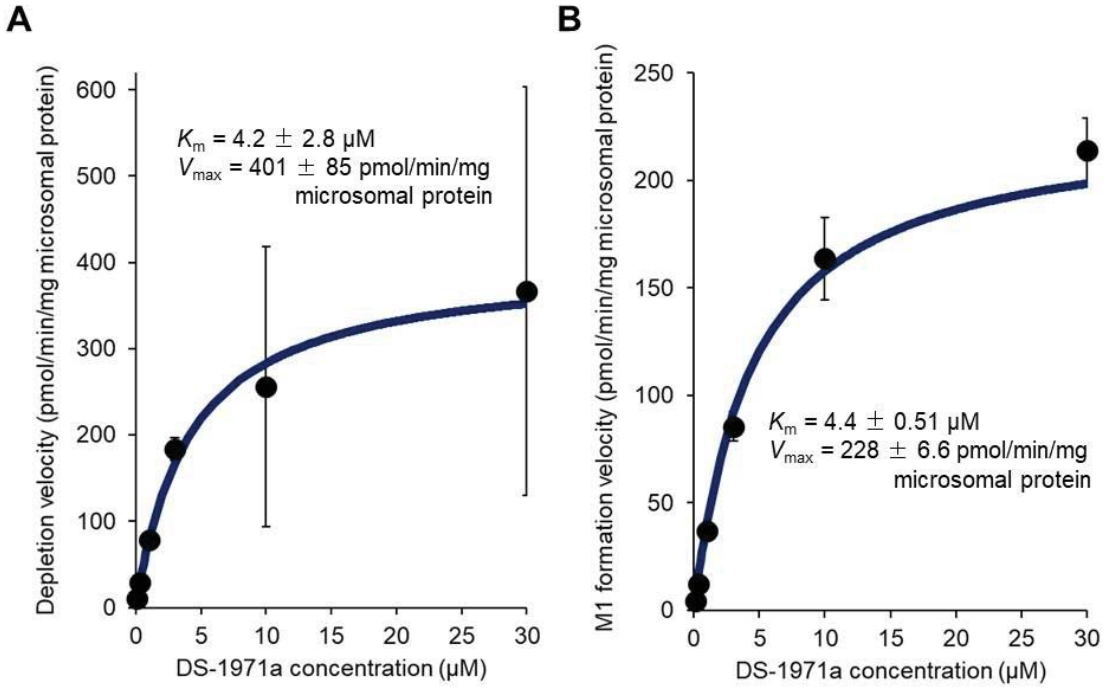

Fig. 4.

DMD Fast Forward. Published on October 23, 2022 as DOI: 10.1124/dmd.122.001000
This article has not been copyedited and formatted. The final version may differ from this version.

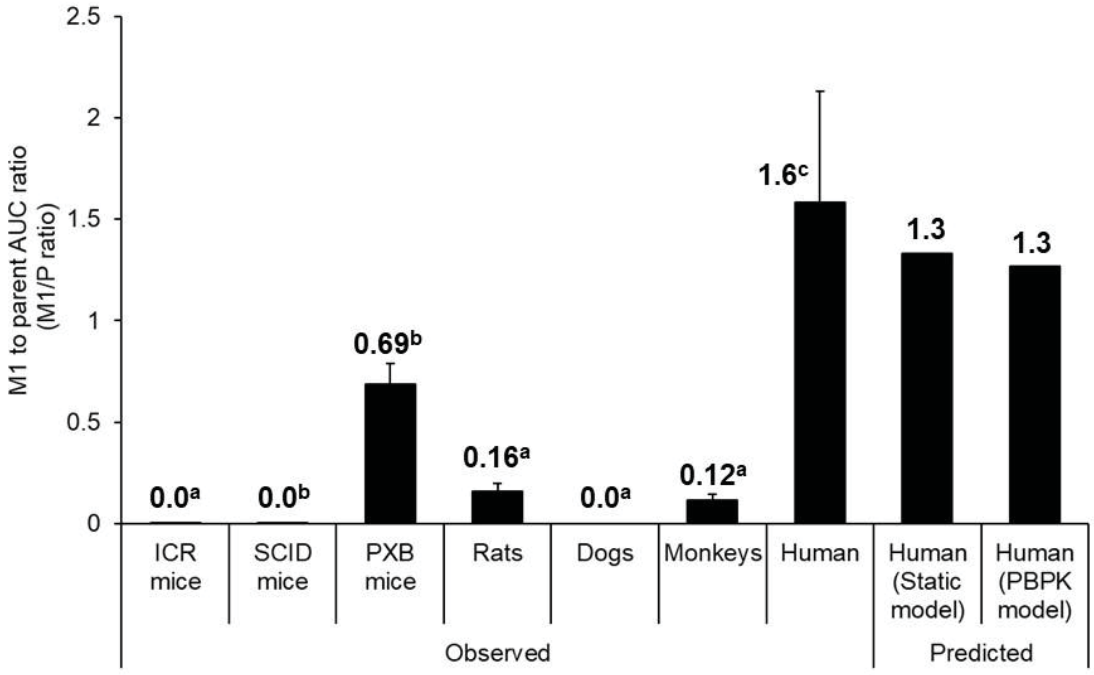

Fig. 5.

DMD Fast Forward. Published on October 23, 2022 as DOI: 10.1124/dmd.122.001000
This article has not been copyedited and formatted. The final version may differ from this version.

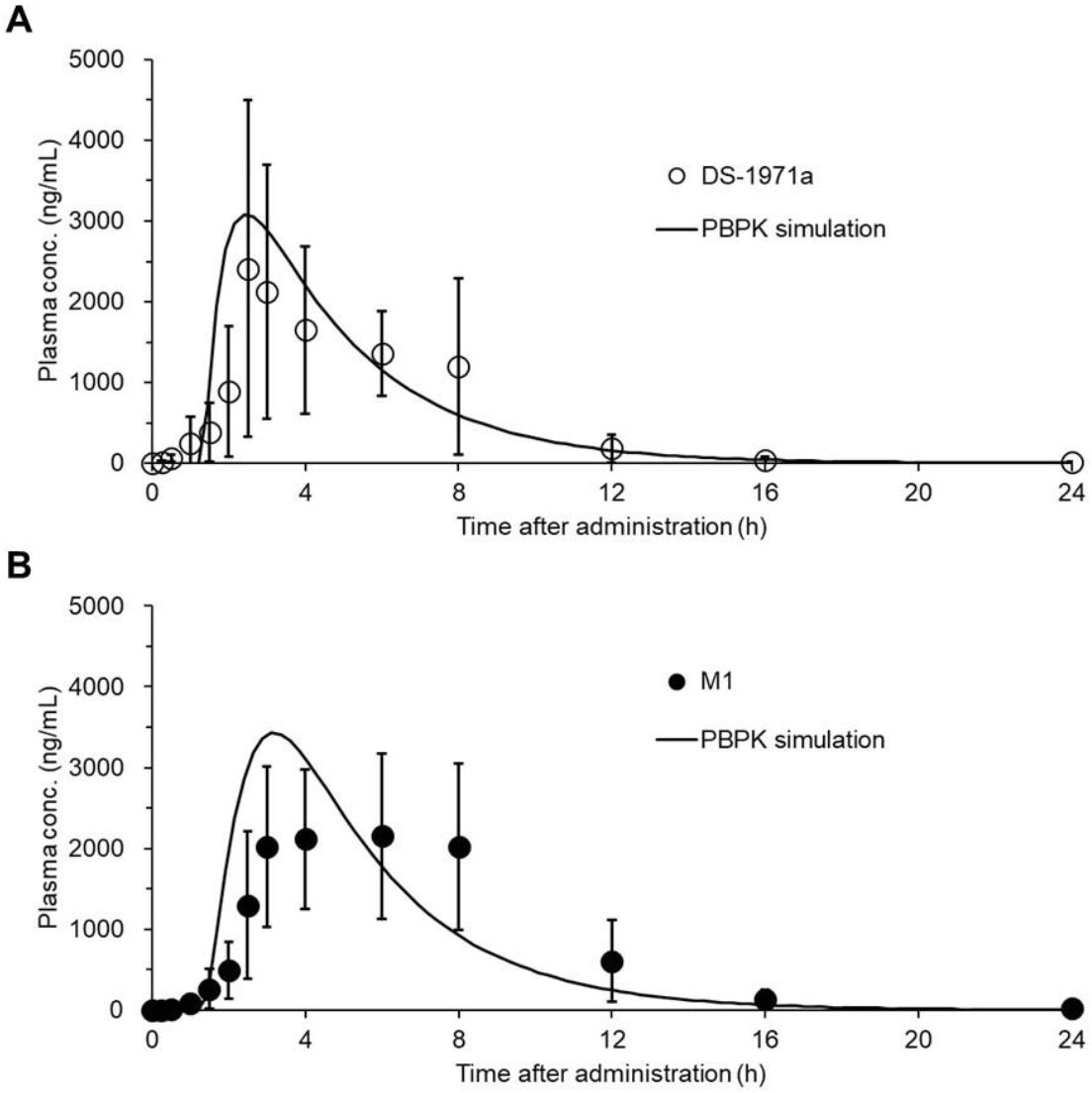

Fig. 6.

Drug Metabolism and Disposition
Manuscript number: DMD-AR-2022-001000

Title page

Physiologically based pharmacokinetic modeling for quantitative prediction of exposure to a human disproportionate metabolite of the selective $Na_V1.7$ inhibitor DS-1971a, a mixed substrate of cytochrome P450 and aldehyde oxidase, using chimeric mice with humanized liver

Daigo Asano, Koichi Nakamura, Yumi Nishiya, Hideyuki Shiozawa, Hideo Takakusa, Takahiro Shibayama, Shin-ichi Inoue, Tsuyoshi Shinozuka, Takakazu Hamada, Chizuko Yahara, Nobuaki Watanabe, Kouichi Yoshinari

Affiliations

Drug Metabolism and Pharmacokinetics Research Laboratories, Daiichi Sankyo Co., Ltd., Tokyo, Japan (D.A., K.N., N.Y., H.S., H.T., T. Shibayama, S.I., C.Y., N.W.), R&D Planning & Management Department, Daiichi Sankyo Co., Ltd., Tokyo, Japan (T. Shinozuka), Research function, Daiichi Sankyo Co., Ltd., Tokyo, Japan (T.H.), Laboratory of Molecular Toxicology, School of Pharmaceutical Sciences, University of Shizuoka, Shizuoka, Japan (K.Y.)

Supplemental Data

Supplementary Table S1. Plasma PK parameters of DS-1971a and its metabolites in SCID mice and PXB-mice after oral administration of DS-1971a at 10 mg/kg in the fasted condition.

	SCID mice			PXB-mice		
	Plasma T_{max} (h)	Plasma C_{max} (ng/mL)	Plasma AUC (ng·h/mL)	Plasma T_{max} (h)	Plasma C_{max} (ng/mL)	Plasma AUC (ng·h/mL)
DS-1971a	0.25 ± 0.0	3241 ± 145	1736 ± 191	0.25 ± 0.0	5327 ± 433	5113 ± 548
M1	0.25 ± 0.0	8.8 ± 3.2	5.7 ± 1.6	0.42 ± 0.14	1684 ± 232	3472 ± 253
M2	0.25 ± 0.0	86 ± 21	113 ± 36	0.42 ± 0.14	946 ± 108	2133 ± 141
M3	0.33 ± 0.14	9.5 ± 3.8	8.5 ± 4.4	0.50 ± 0.0	350 ± 32	682 ± 6.0
M4	0.50 ± 0.0	943 ± 117	941 ± 104	0.50 ± 0.0	35 ± 4.5	54 ± 7.5
M7	0.83 ± 0.29	119 ± 14	171 ± 26	0.83 ± 0.29	26 ± 6.4	28 ± 5.0
M8	0.67 ± 0.29	251 ± 23	307 ± 69	1.0 ± 0.0	127 ± 48	378 ± 69
M9	0.67 ± 0.29	13 ± 2.0	15 ± 1.6	0.67 ± 0.29	86 ± 28	162 ± 56

PK parameters were calculated based on the concentrations determined in plasma, which were collected at 0.25, 0.5, 1, 2, 4, 7, and 24 h after oral administration of DS-1971a (10 mg/kg) using non-compartmental analysis. Each value represents the mean ± SD of three mice.

Supplementary Table S2. Plasma PK parameters of DS-1971a and M1 after intravenous and/or oral administration of DS-1971a or M1 to SCID mice and/or PXB-mice in the fasted condition.

Mice	Dosing compound	i.v.		p.o.		
		Plasma Vd_{ss} (L/kg)	Plasma *CL* (mL/min/kg)	Plasma C_{max} (ng/mL)	Plasma AUC (ng·h/mL)	Oral bioavailability (%)
SCID	DS-1971a	0.98 ± 0.10	48 ± 5.8	3241 ± 145	1736 ± 191	49 ± 5.4
PXB	DS-1971a	0.34 ± 0.048	20 ± 4.5	5327 ± 433	5113 ± 548	60 ± 6.4
	M1	0.23 ± 0.024	11 ± 4.4	NA	NA	NA

PK parameters were calculated based on the concentrations determined in plasma, which were collected at 0.083 and/or 0.25, 0.5, 1, 2, 4, 7, and 24 h after intravenous (i.v.) and/or oral (p.o.) administration of DS-1971a or M1 using non-compartmental analysis. Each value represents the mean ± SD of three mice. NA, not applicable.

Supplementary Table S3. Observed PBPK parameters of DS-1971a and M1 in PXB-mice.

Parameters		DS-1971a	M1	Source	Static model	PBPK model
Molecular weight		465	481	-	×	×
Plasma distribution volume at steady state: Vd_{ss} (L/kg)		0.34	0.23	Measured		
Detail	Blood-based extrahepatic distribution volume: $V1p$[a] or $V1m$[a] (L)	0.0079[a]	0.0060[a]	Calculated[a]		×
	Liver volume: Vh (L)	0.0013		Reported (Davies and Morris, 1993)		×
	Liver to plasma ratio: Kphp and Kphm	3.2	1.1	Measured		×
fCL,m[b] (ratio)		0.25[b]	-	Measured[b]	×	×
Total plasma clearance: CLp,total or CLm,total (mL/min/kg)		20	11	Measured (Supplementary Table S2)	×	
Detail	Metabolic plasma clearance: CLmp[c] or CLmm[d] (mL/min/kg)	20[c]	0.0[d]	Calculated[c, d]	×	×
	Biliary plasma clearance: CLbp[e] or CLbm[f] (mL/min/kg)	0.27[e]	4.6[f]	Measured[e, f]	×	×
	Renal plasma clearance: CLrp[g] or CLrm[h] (mL/min/kg)	0.14[g]	7.1[h]	Measured[g, h]		×
Hepatic bioavailability: Fh,p[i] or Fh,m[j]		0.59[i]	0.91[j]	Calculated[i, j]	×	
Plasma M1/ P ratio[k] by the static model		0.72[k]		Calculated[k]	×	

a: eq. (31), b: fCL,m in PXB-mice was the cumulative recovery of M1 into urine and feces, c: eq. (6), d: eq. (7), e: eq. (2), f: eq. (3), g: eq. (4), h: eq. (5), i: eq. (10), j: eq. (11), k: eq. (13). Note that [d]CLmm was regarded as 0 because CLm,total was almost equal to [CLbm + CLrm].

Supplementary Table S4. Inputted parameters in the PBPK model for PXB-mice.

Inputted parameter	Explanation	Value	Unit	Source
Dose	Oral dose	0.20	mg	Oral administration of 10 mg/kg to mice with body weight of 20 g
*F*a	Fraction absorbed	1.0		Reported (Asano et al., 2021)
*F*g	Intestinal availability	1.0		Calculated
Ag1	Drug amount in upper intestine	Variable	mg	-
Ag2	Drug amount in lower intestine	Variable	mg	
*V*h	Liver volume	0.0013	L	Reported (Davies and Morris, 1993)
*Q*h	Liver blood flow	90	mL/min/kg	
*k*a1	Absorption constant in upper intestine	2.8 ± 0.6	h^{-1}	Obtained by fitting DS-1971a PK to the PBPK model using Winnonlin 6.3.
*k*a2	Absorption constant in lower intestine	0.22 ± 0.01	h^{-1}	
*k*t	Transit constant in gastrointestinal tract	1.8 ± 0.5	h^{-1}	
MWp and MWm	Molecular weight of DS-1971a and M1	465, 481	g/mole	Calculated
*R*bp and *R*bm	Blood-to-plasma concentration ratio of DS-1971a and M1	0.55, 0.56	-	Measured
*f*up and *f*um	Unbound fraction of DS-1971a and M1 in plasma	0.010, 0.020	-	Reported (Sinozuka et al., 2020; Asano et al., 2022)
Chp and Chm	Hepatic concentration of DS-1971a and M1	Variable	ng/mL	-
*K*php and *K*phm	Liver-to-plasma ratio of DS-1971a and M1	3.2, 1.1	-	Measured (Supplementary Table S3)
Cbp and Cbm	Blood concentration of DS-1971a and M1	Variable	ng/mL	-
*V*1p and *V*1m	Blood-based extrahepatic distribution volume of DS-1971a and M1	0.0079, 0.0060	L	Calculated (Supplementary Table S3)
CL_{int},bp[a] and CL_{int},bm[b]	Biliary blood intrinsic clearance of DS-1971a and M1	0.032[a], 0.30[b]	L/h	Calculated[a, b]
blood-*CL*rp[c] and -*CL*rm[d]	Renal blood clearance of DS-1971a and M1	0.00030[c], 0.015[d]	L/h	Calculated[c, d]
f*CL*,m	Fraction of the clearance of DS-1971a that yields M1	0.25	-	Measured (Supplementary Table S3)
CL_{int},mp[e]	Metabolic blood intrinsic clearance of DS-1971a	4.0[e]	L/h	Calculated[e]

a: eq. (26), b: eq. (25), c: eq. (23), d: eq. (24), e: eq. (27)

Supplementary Table S5. Observed and PBPK model-simulated plasma PK parameters for PXB-mice after oral administration of DS-1971a at 10 mg/kg in the fasted condition.

Compounds	Method	Plasma C_{max} (ng/mL)	Plasma AUC (ng·h/mL)	Plasma M1/P ratio
DS-1971a	Dynamic PBPK simulation	4728	4924	-
	Observed[a]	5327 ± 433[a]	5113 ± 548[a]	-
M1	Dynamic PBPK simulation	2183	3339	0.68
	Observed[a]	1684 ± 232[a]	3472 ± 253[a]	0.69 ± 0.10[a]

a: Data represent the mean ± SD of three mice.

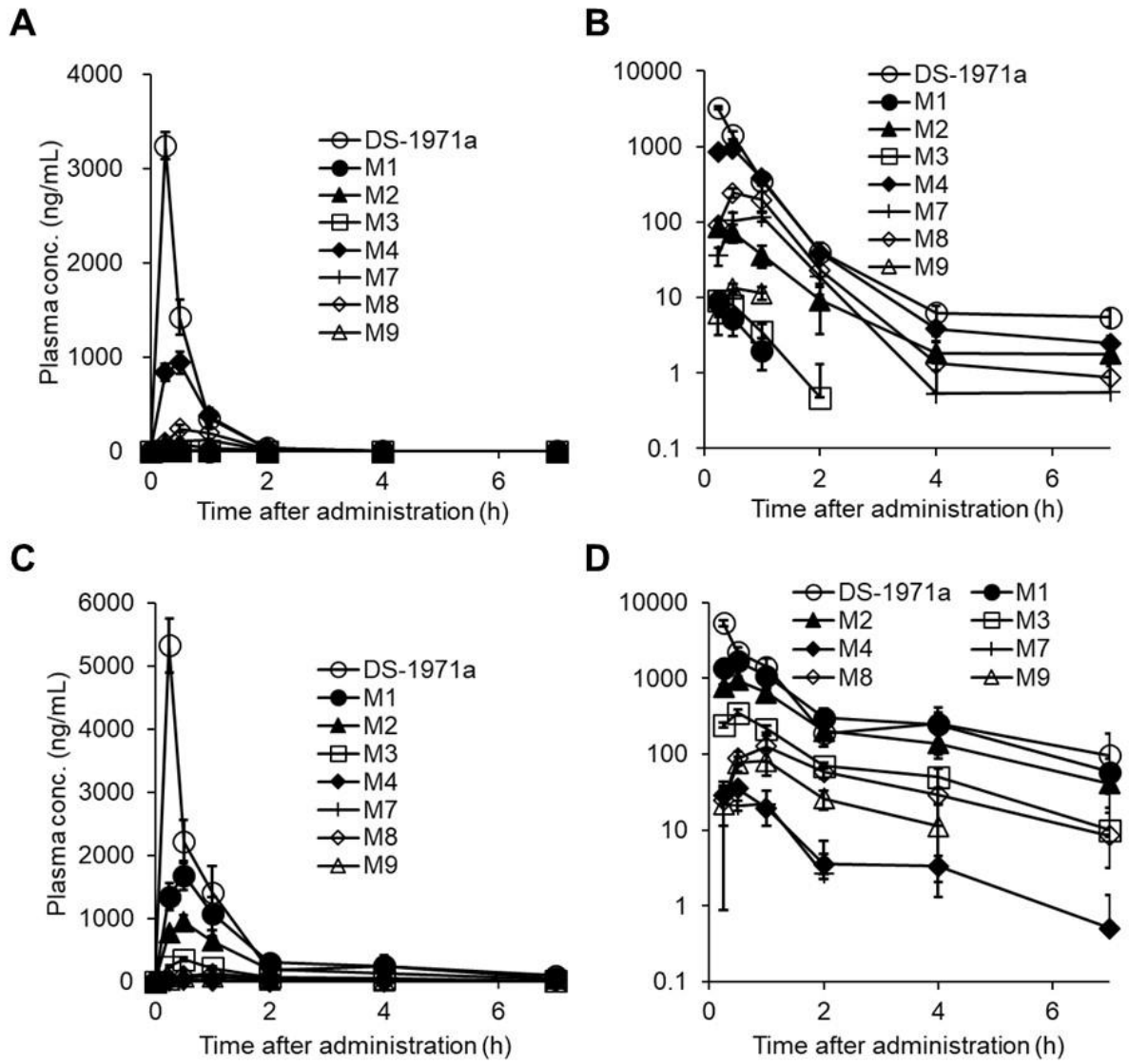

Supplementary Fig. S1. Time-dependent changes in the plasma concentrations of DS-1971a and its metabolites in the plasma obtained from SCID mice (A and B) and PXB-mice (C and D) after oral administration of DS-1971a at 10 mg/kg in the fasted condition. Plasma concentrations of DS-1971a and its metabolites were determined by LC-MS/MS and plotted. Each point represents the mean ± SD of three mice. A and C, linear plot; B and D, semilog plot.

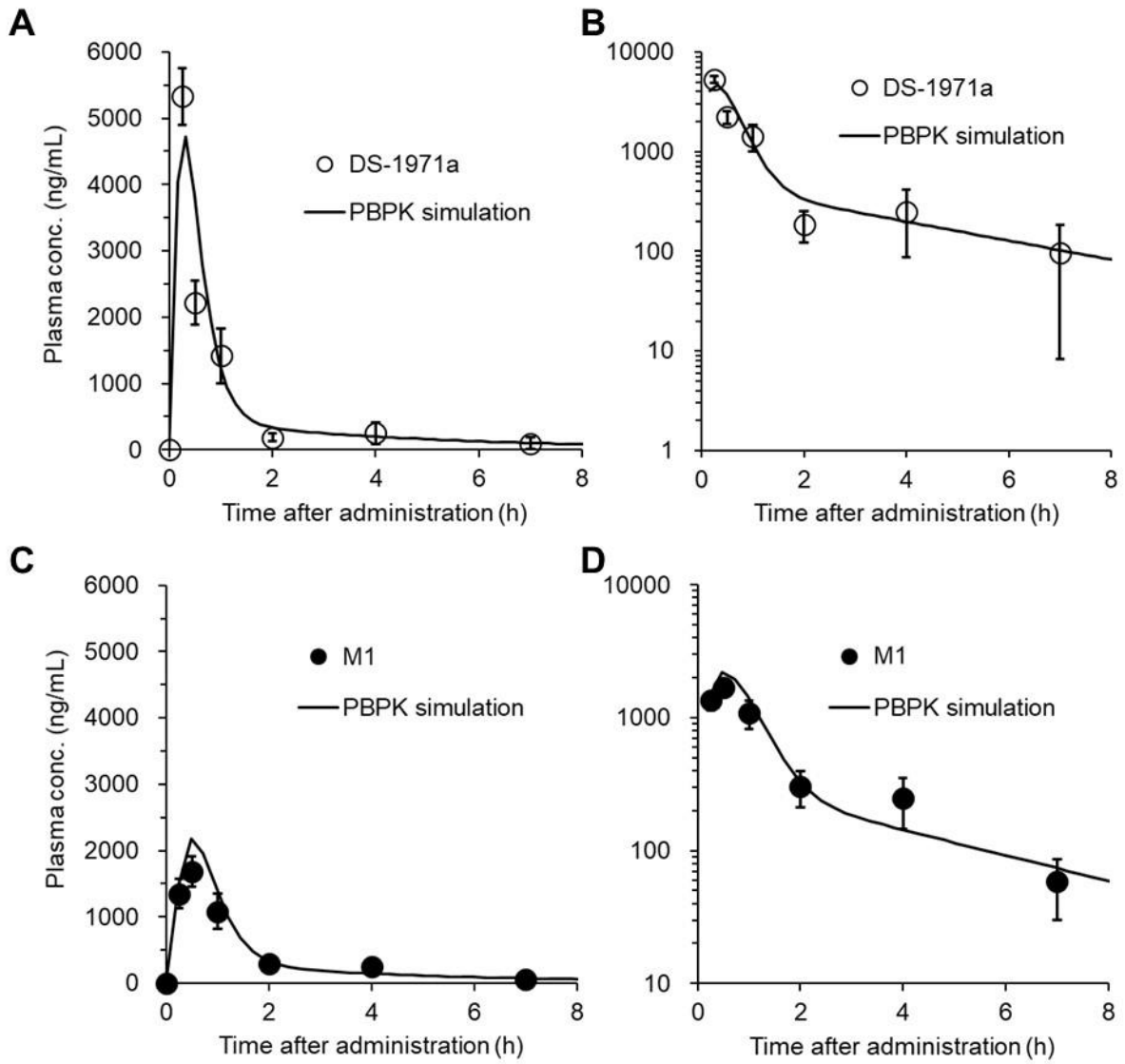

Supplementary Fig. S2. Simulated plasma PK profiles of DS-1971a (A and B) and M1 (C and D) in PXB-mice after oral administration of DS-1971a at 10 mg/kg in the fasted condition using the dynamic PBPK model.

PBPK modeling was performed based on the customized model (Fig. 2) and parameters shown in Supplementary Table S4 using WinNonlin 6.3. Open and closed circles represent the observed plasma concentrations (mean ± SD of three mice) of DS-1971a and M1, respectively (Asano et al., 2022). Solid line indicates the simulated PK profiles of DS-1971a and M1 by the dynamic PBPK model. A and C, linear plot; B and D, semilog plot.

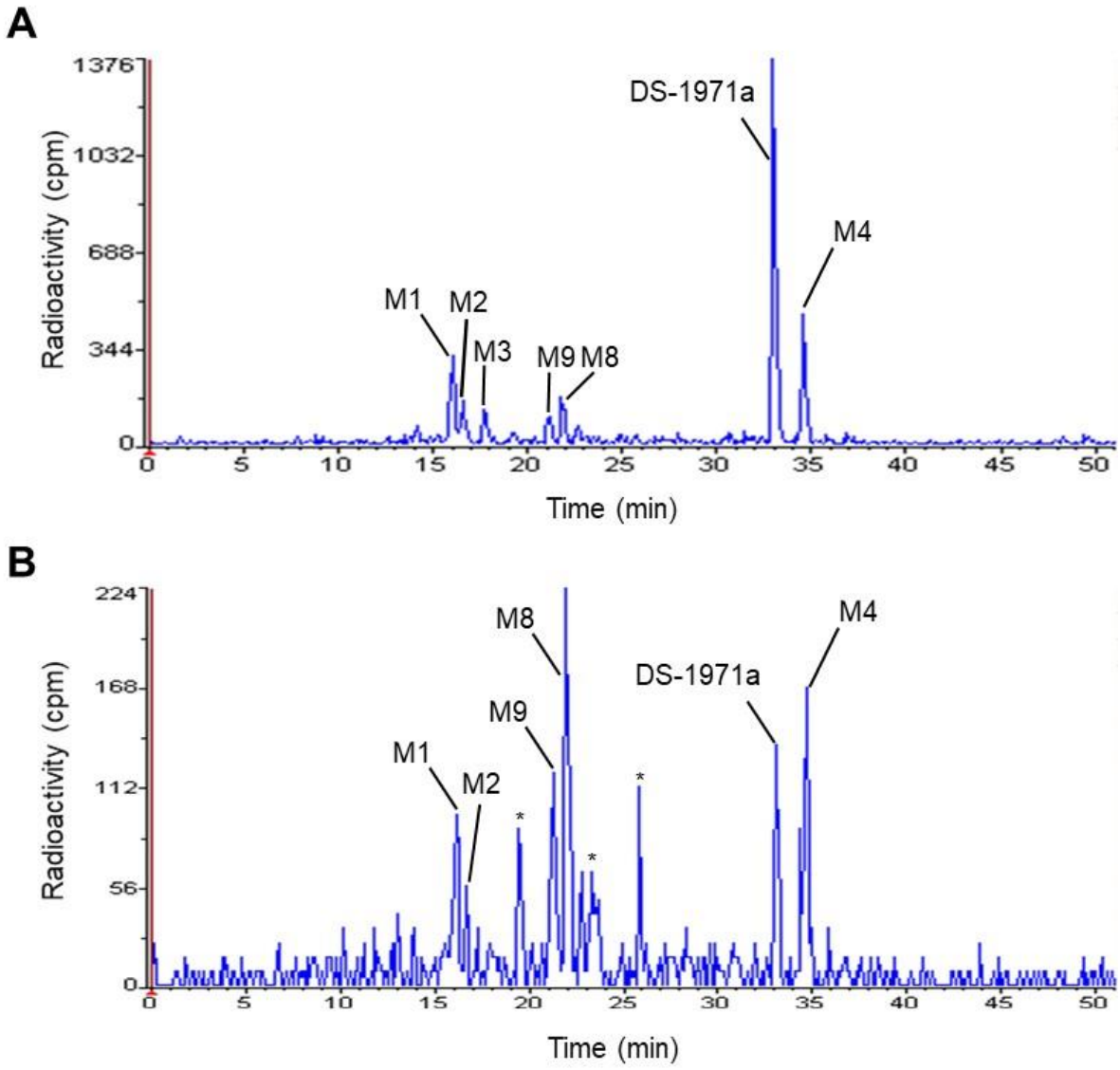

Supplementary Fig. S3. Radiochromatograms of metabolites in (A) PXB cells incubated with DS-1971a at 1 μM and (B) the liver from PXB-mice after oral administration of DS-1971a at 10 mg/kg in the fasted condition.

PXB cells (A) incubated for 2 h with [^{3}H]DS-1971a at 37°C and 5% CO_2, and liver (B) obtained from PXB-mice at 1 h after [^{3}H]DS-1971a administration were analyzed using radio-HPLC. The radioactive peaks of the parent and metabolites were identified by comparing their retention times with those of authentic standards for the parent and each metabolite. * indicates unknown metabolites.

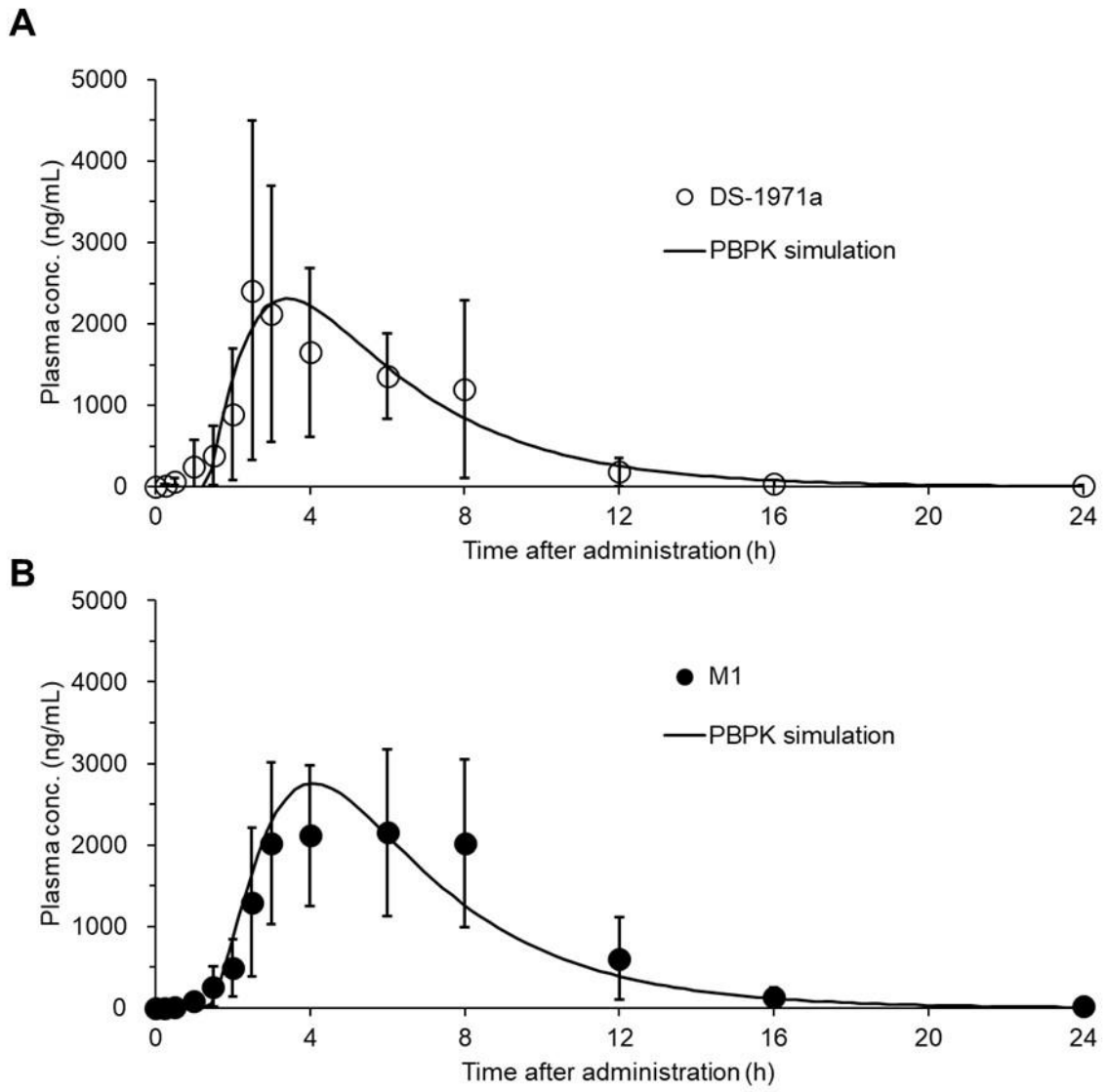

Supplementary Fig. S4. The simulated plasma PK profiles of DS-1971a (A) and M1 (B) in humans with the optimized *k*a1, *k*a2, and *k*t values after oral administration of DS-1971a at 400 mg in the fed condition using the dynamic PBPK model.

Supplementary PBPK modeling was performed based on the customized model (Fig. 2) with the replacement of *k*a1, *k*a2, and *k*t values (0.33, 0.33, and 0.57 h^{-1}) in Table 5 by the fitted supplementary values (0.088, 0.30, and 0.89 h^{-1}, respectively) using WinNonlin 6.3. Open and closed circles represent the observed plasma concentrations of DS-1971a and M1 (mean ± SD of six humans), respectively (Asano et al., 2022). Solid line indicates the simulated PK profiles of DS-1971a and M1 by the dynamic PBPK model.